marine drugs

Supplementary Information

New Deoxyenhygrolides from *Plesiocystis pacifica* Provide Insights into Butenolide Core Biosynthesis

Joachim J. Hug [1,2,3†], Louise Kjaerulff [1,2†], Ronald Garcia[1,2,3] and Rolf Müller [1,2,3] *

1 Helmholtz-Institute for Pharmaceutical Research Saarland (HIPS), Helmholtz Centre for Infection Research (HZI), Saarland University, Campus E8 1, 66123 Saarbrücken, Germany; Joachim.Hug@helmholtz-hips.de (J.J.H.), Louisek@sund.ku.dk (L.K.), Ronald.Garcia@helmholtz-hips.de (R.G.).

2 German Center for Infection Research (DZIF), Partner Site Hannover-Braunschweig, Germany

3 Helmholtz International Labs, Department of Microbial Natural Products, Saarland University, Campus E8 1, 66123 Saarbrücken, Germany

* Correspondence: rolf.mueller@helmholtz-hips.de

† These authors contributed equally to this work.

Table of contents

1. MS spectra

1.1 Preparative LC-MS chromatograms

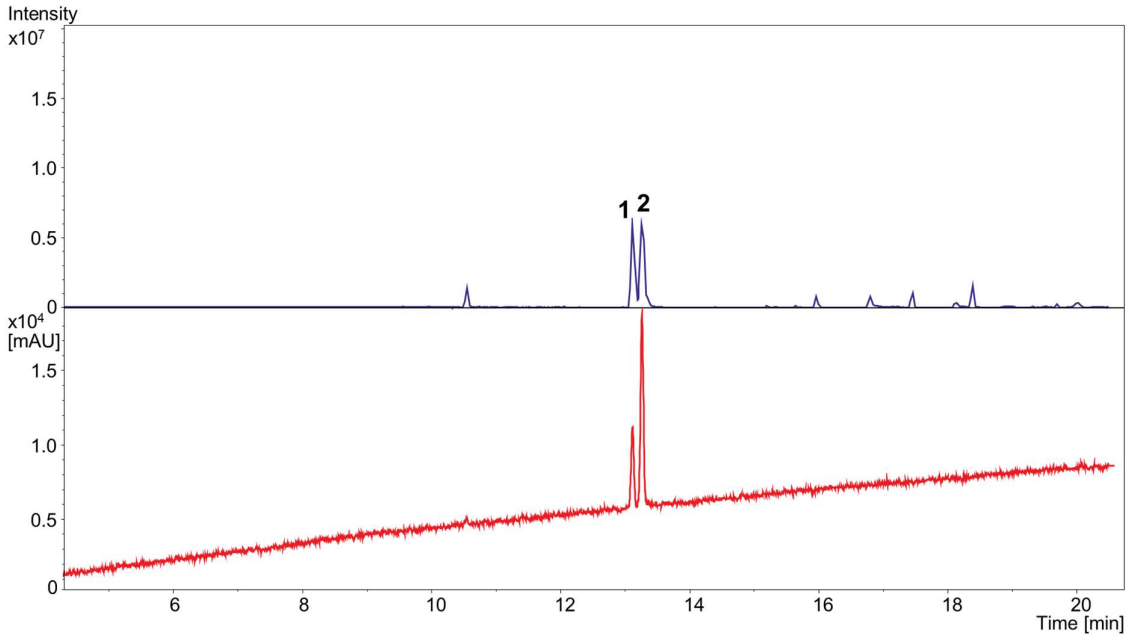

Figure S1. HPLC-MS BPC trace of purified **1** and **2** (top, blue) and UV/VIS (bottom, red) trace of **1** and **2**. Mass spectrum was acquired from 150–2000 *m/z*, in positive mode; UV/VIS detection by a DAD at 200–600 nm.

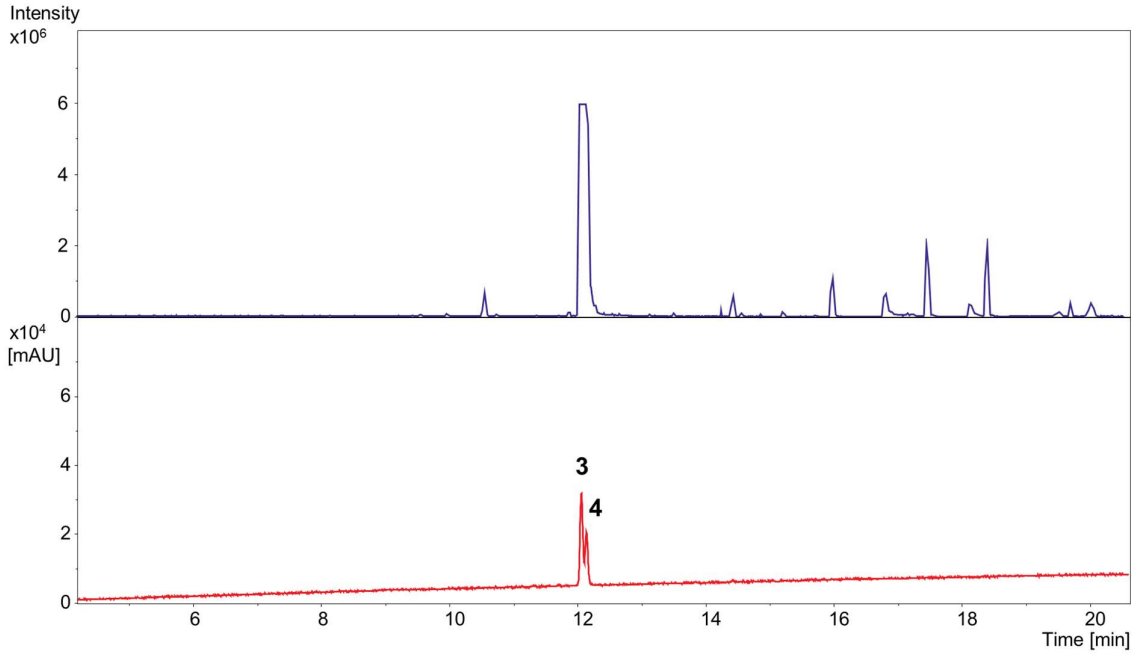

Figure S2. HPLC-MS BPC trace of purified **3** and **4** (top, blue) and UV/VIS (bottom, red) trace of **3** and **4**. Mass spectrum was acquired from 150–2000 *m/z*, in positive mode; UV/VIS detection by a DAD at 200–600 nm.

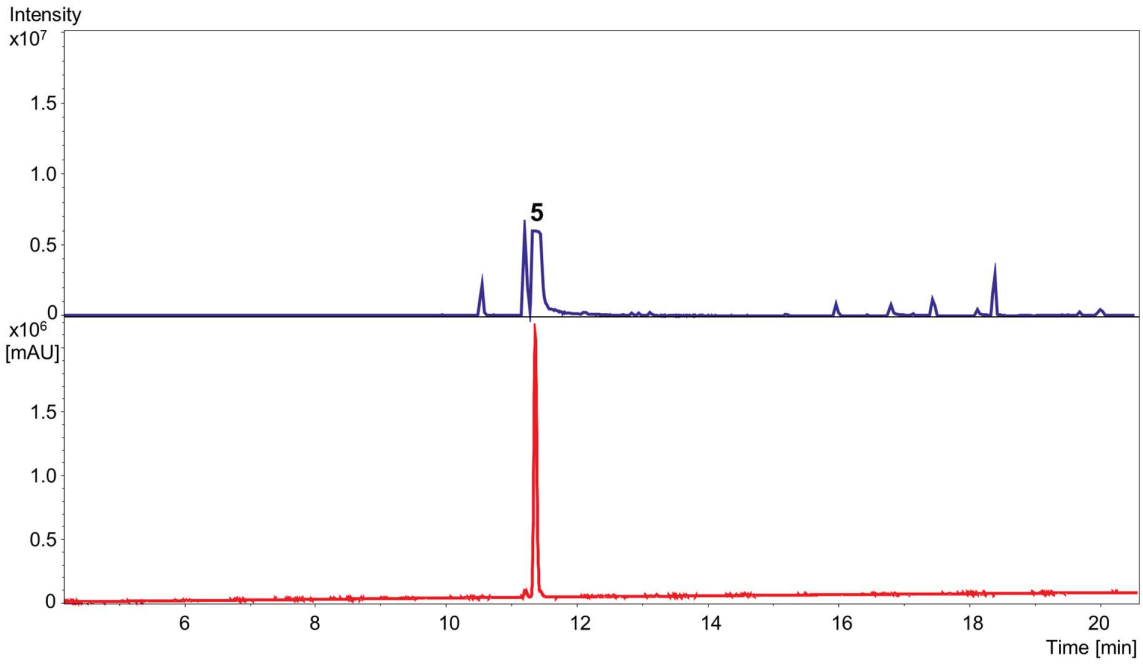

Figure S3. HPLC-MS BPC trace of purified **5** (top, blue) and UV/VIS (bottom, red) trace of **5**. Mass spectrum was acquired from 150–2000 *m*/*z*, in positive mode; UV/VIS detection by a DAD at 200–600 nm.

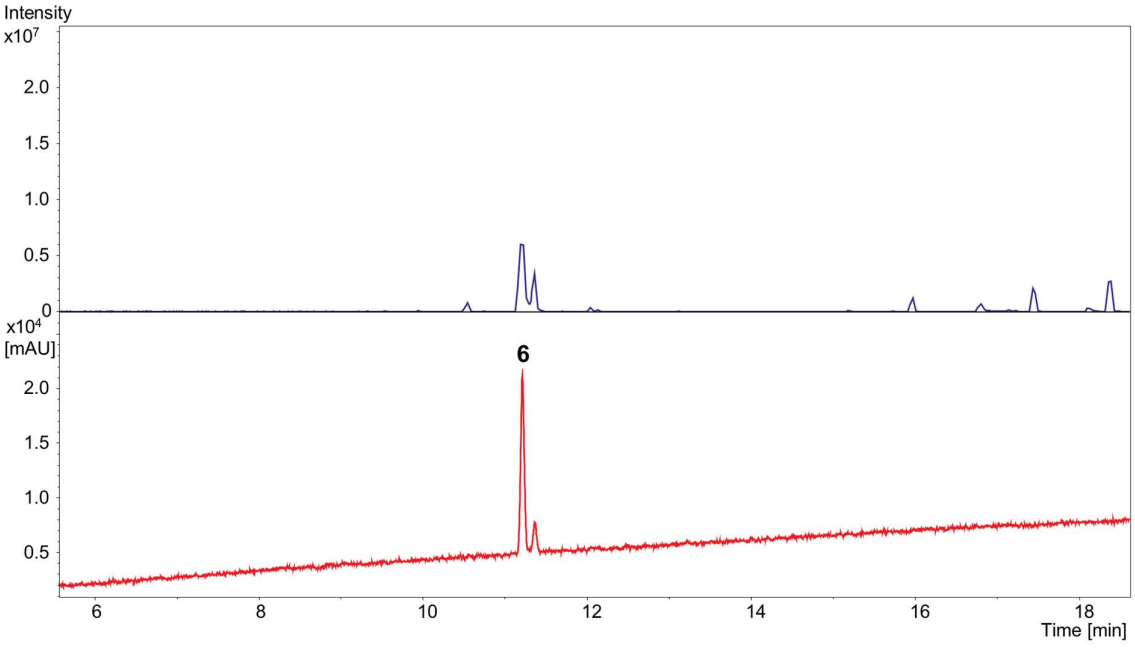

Figure S4. HPLC-MS BPC trace of purified **6** (top, blue) and UV/VIS (bottom, red) trace of **6**. Mass spectrum was acquired from 150–2000 *m*/*z*, in positive mode; UV/VIS detection by a DAD at 200–600 nm.

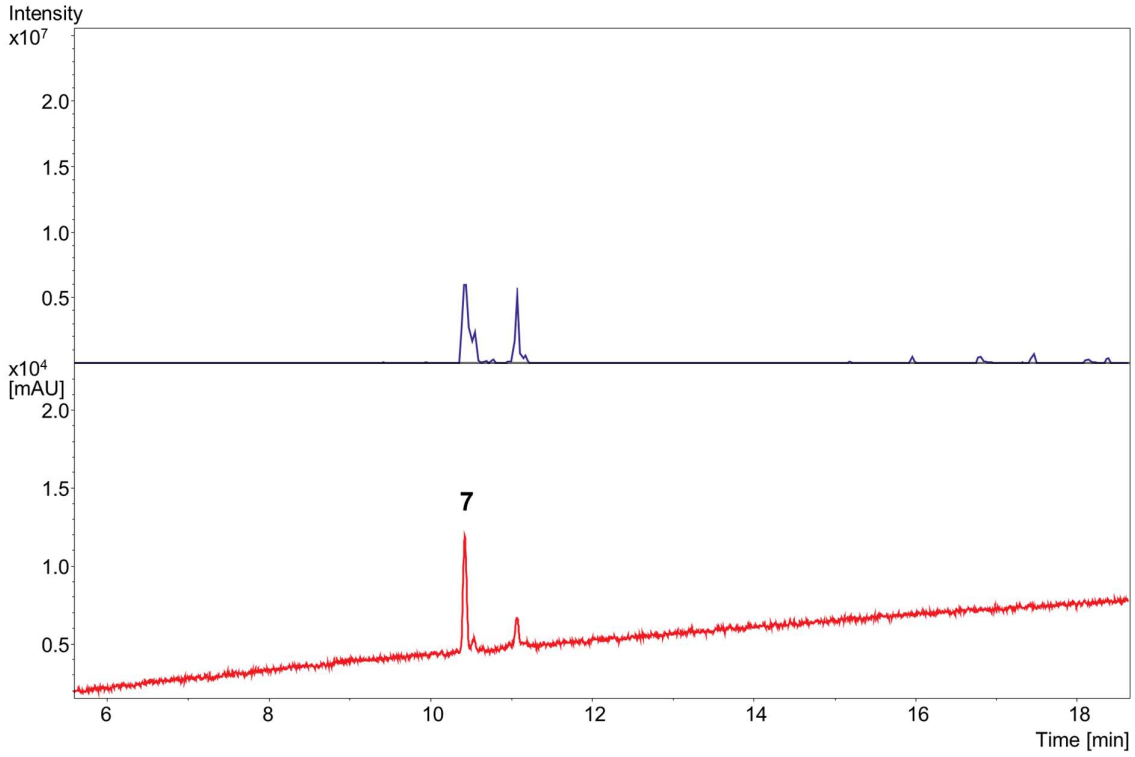

Figure S5. HPLC-MS BPC trace of purified **7** (top, blue) and UV/VIS (bottom, red) spectrum of **7**. Mass spectrum was acquired from 150–2000 *m/z*, in positive mode; UV/VIS detection by a DAD at 200–600 nm.

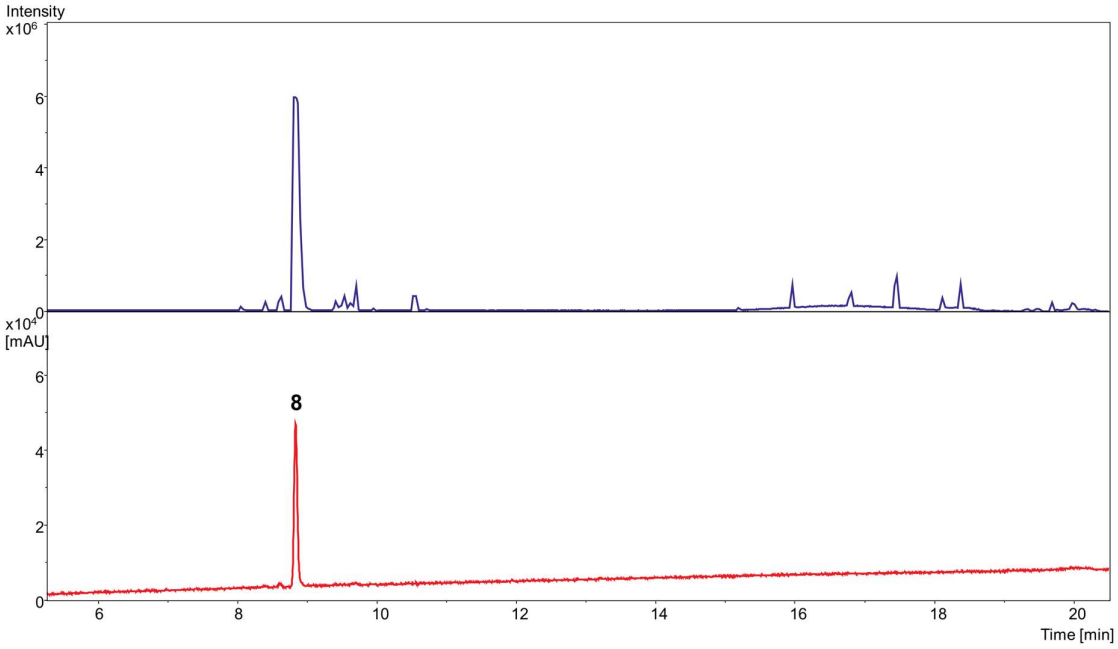

Figure S6. HPLC-MS BPC trace of purified **8** (top, blue) and UV/VIS (bottom, red) spectrum of **8**. Mass spectrum was acquired from 150–2000 *m/z*, in positive mode; UV/VIS detection by a DAD at 200–600 nm.

1.2 Partial ESI-MS spectra

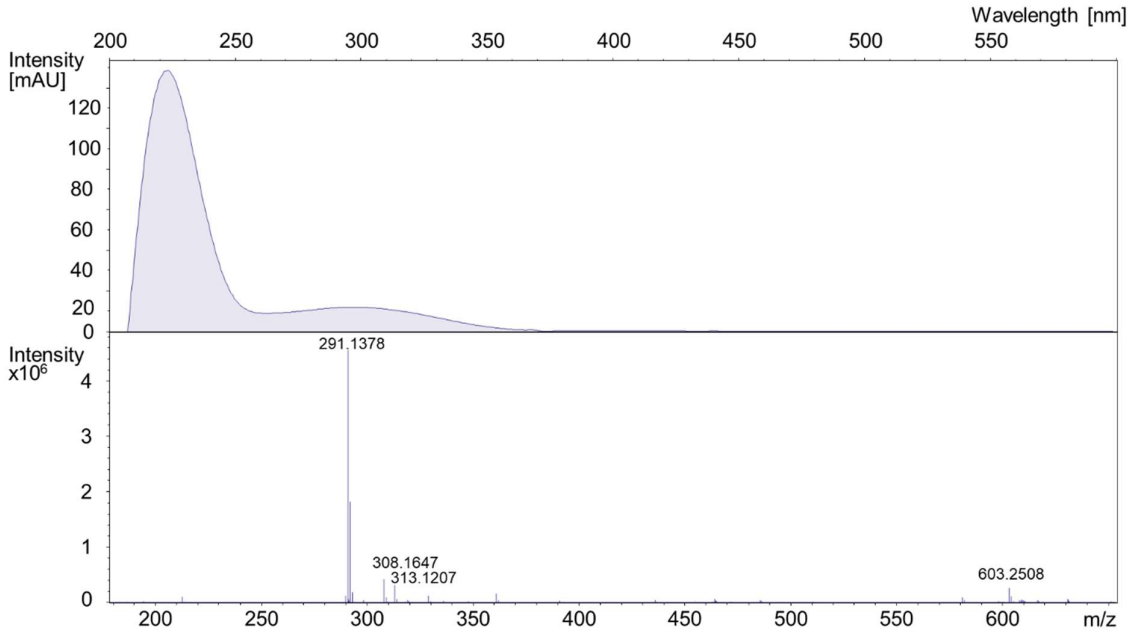

Figure S7. UV/VIS and partial ESI+MS spectra of purified **1** (291.1378 $[M+H]^+$, 308.1647 $[M+NH_4]^+$, 313.1207 $[M+Na]^+$, 603.2508 $[2M+Na]^+$). RT: 13.05–13.15 min.

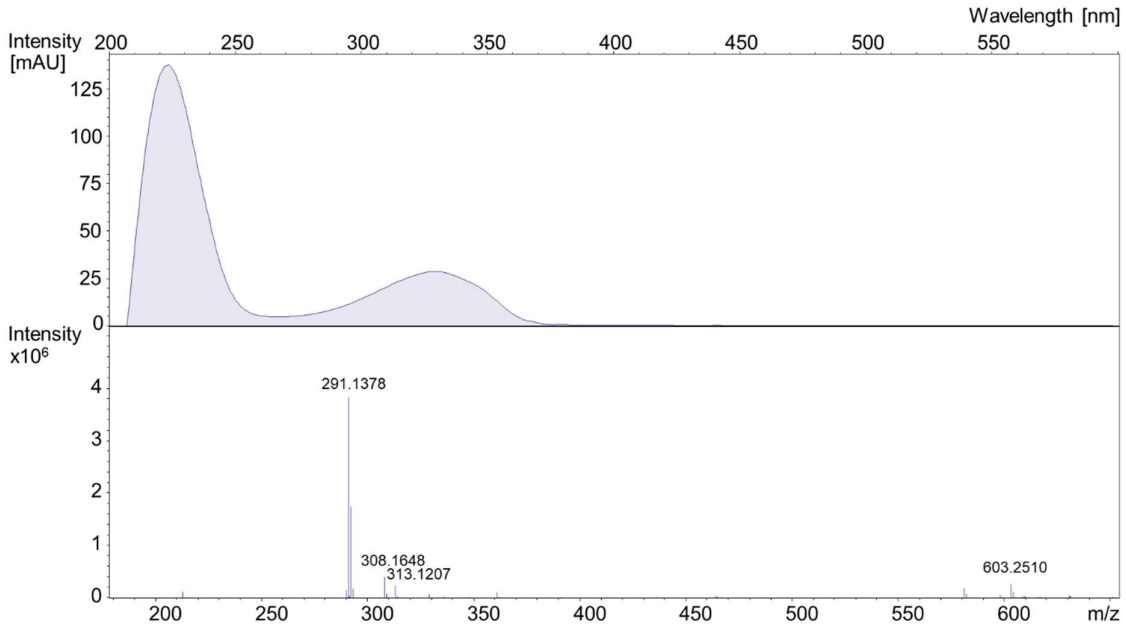

Figure S8. UV/VIS and partial ESI+MS spectra of purified **2**. 291.1378 $[M+H]^+$, 308.1648 $[M+NH_4]^+$, 313.1207 $[M+Na]^+$, 603.2510 $[2M+Na]^+$). RT: 13.20–13.30 min.

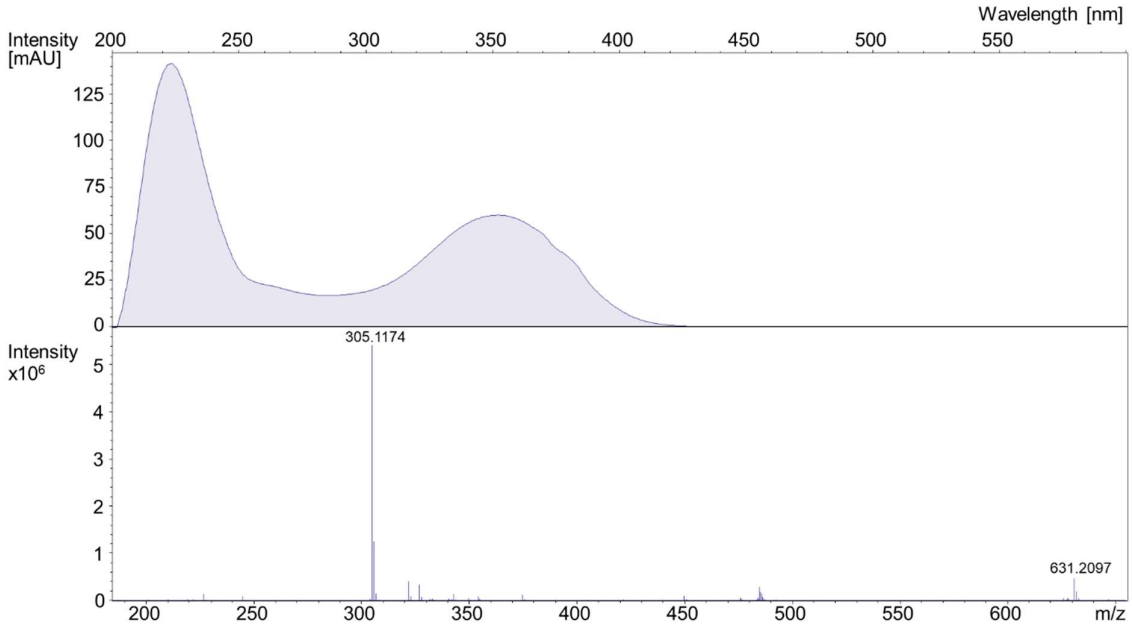

Figure S9. UV/VIS and partial ESI+MS spectra of purified **3**. 305.1174 $[M+H]^+$, 631.2097 $[2M+Na]^+$. RT: 12.00–12.10 min.

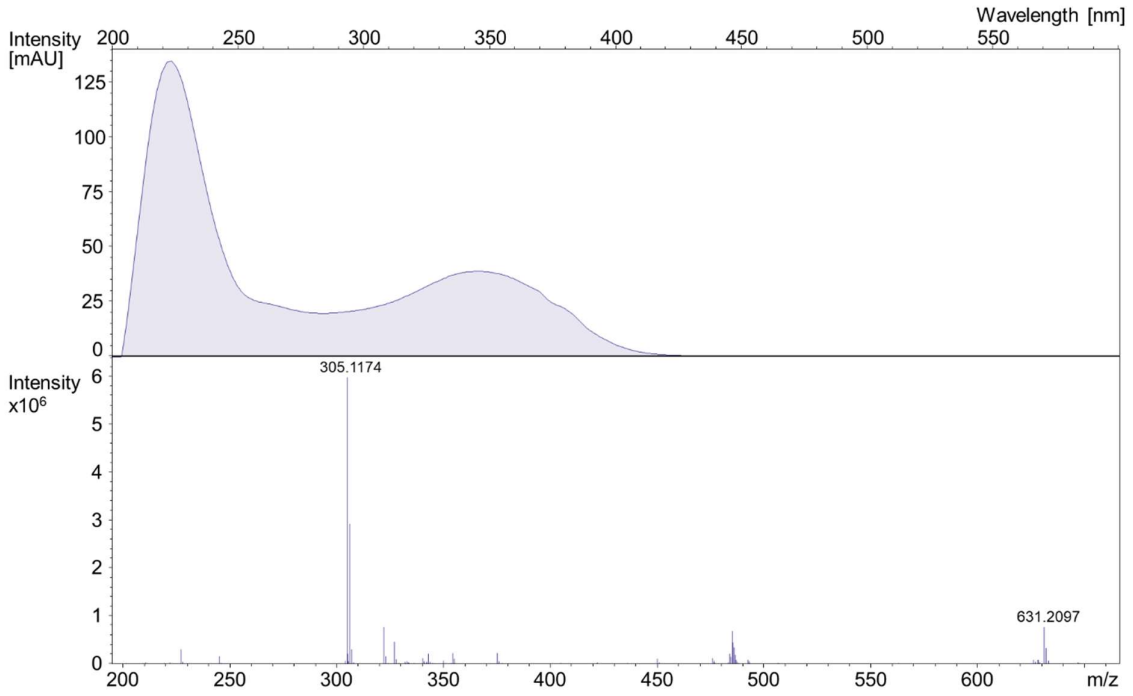

Figure S10. UV/VIS and partial ESI+MS spectra of purified **4**. 305.1174 $[M+H]^+$, 631.2097 $[2M+Na]^+$. RT: 12.10–12.20 min.

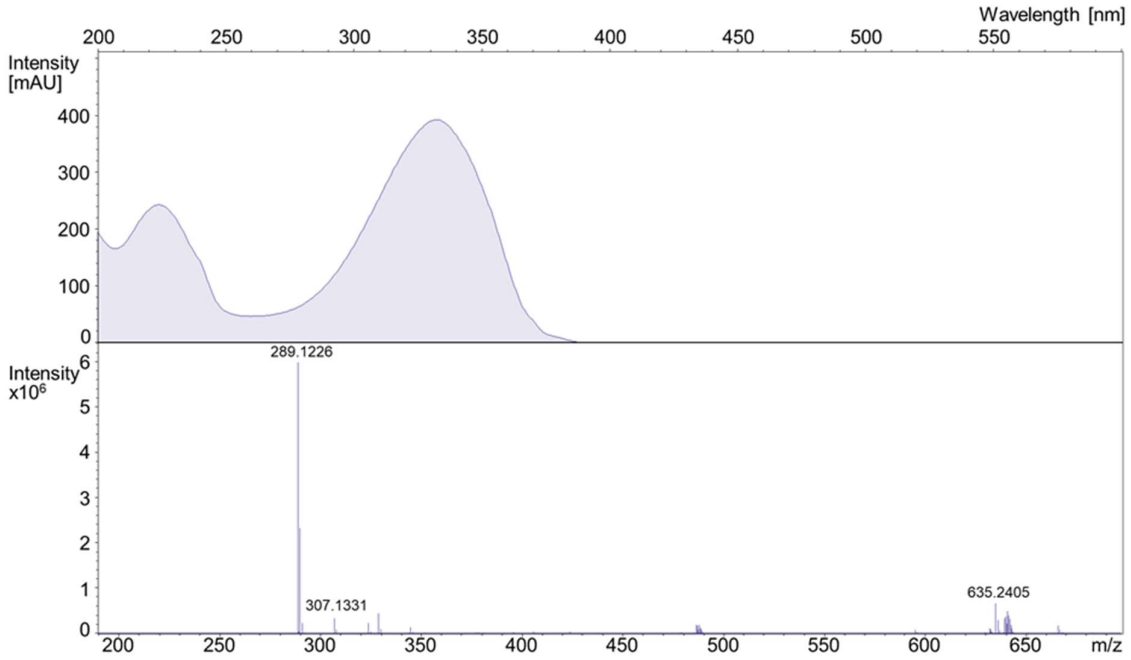

Figure S11. UV/VIS and partial ESI+MS spectra of purified **5**. 289.1243 $[M\text{-}H_2O+H]^+$, 307.1331 $[M+H]^+$, 635.2405 $[2M+Na]^+$. RT: 11.30–11.45 min.

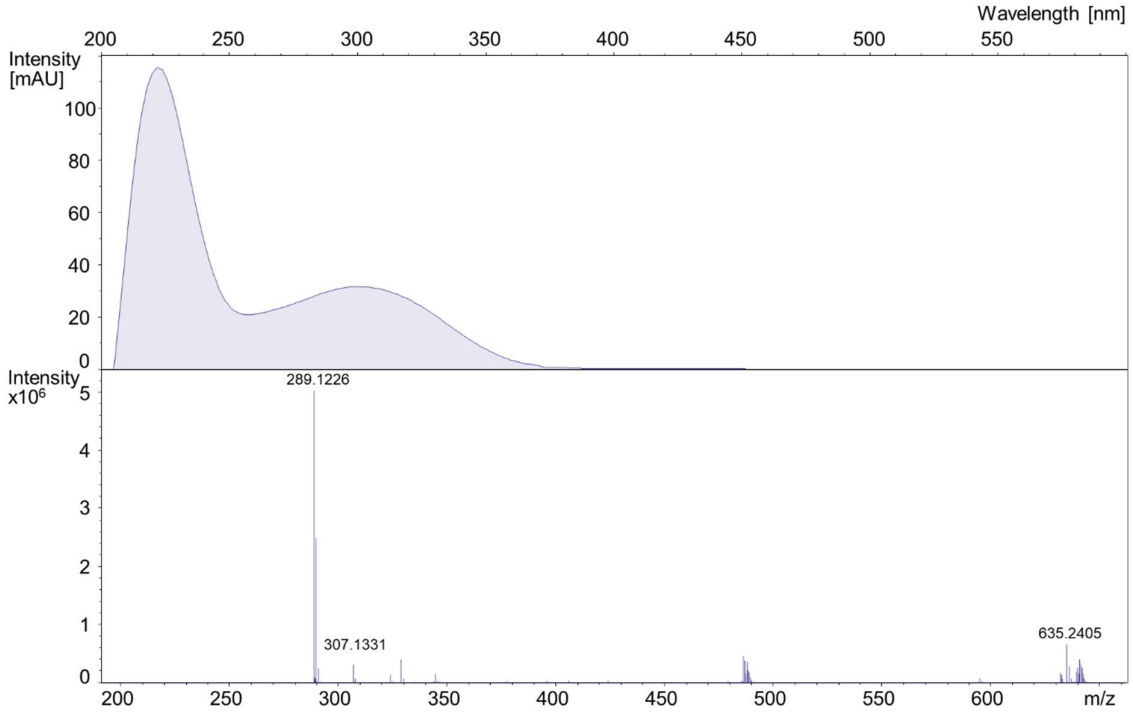

Figure S12. UV/VIS and partial ESI+MS spectra of purified **6**. 289.1226 $[M\text{-}H_2O+H]^+$, 307.1331 $[M+H]^+$, 635.2405 $[2M+Na]^+$. RT: 11.15–11.25 min.

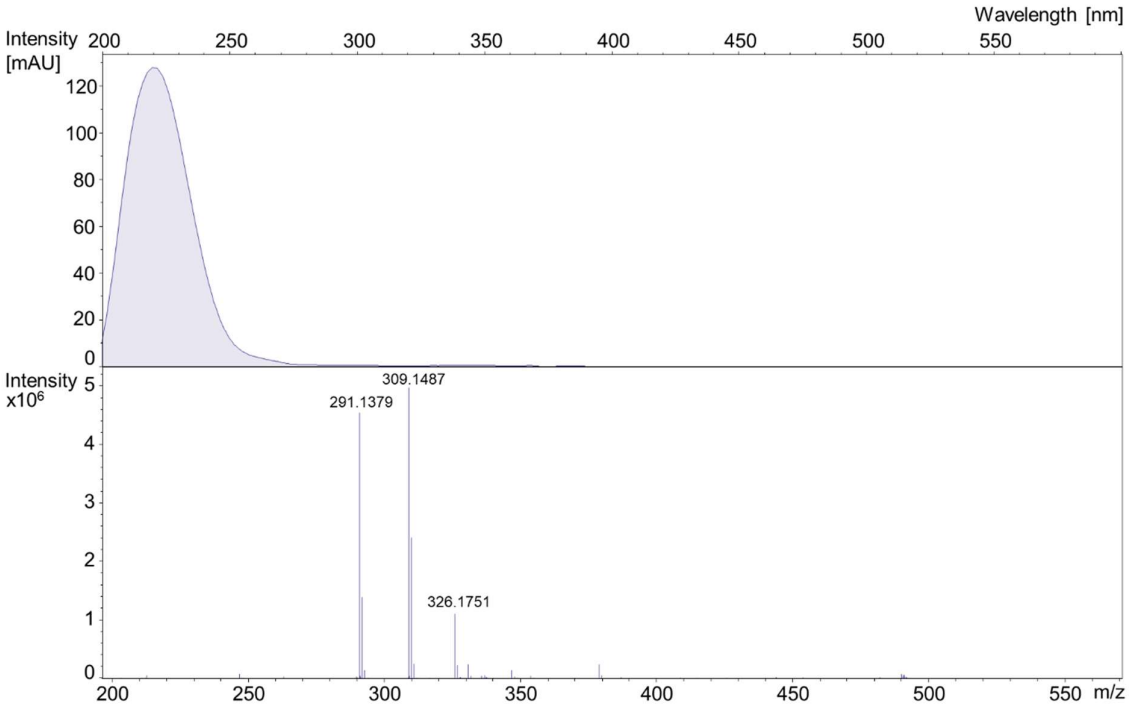

Figure S13. UV/VIS and partial ESI+MS spectra of purified **7**. 291.1379 $[M\text{-}H_2O+H]^+$, 309.1487 $[M+H]^+$, 326.1751 $[M+NH_4]^+$. RT: 10.38–10.48 min.

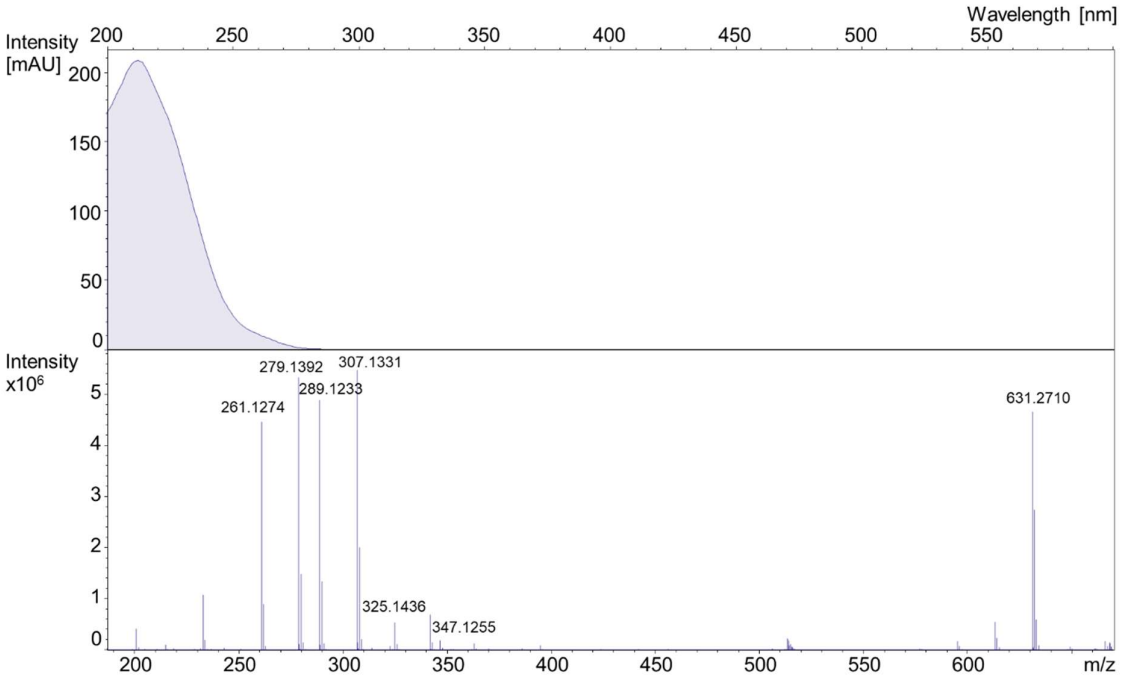

Figure S14. UV/VIS and partial ESI+MS spectra of purified **8**. 289.12332 $[M\text{-}2H_2O+H]^+$, 261.1274 $[M\text{-}2H_2O\text{-}C_2H_4+H]^+$, 307.1331 $[M\text{-}H_2O+H]^+$, 279.1392 $[M\text{-}H_2O\text{-}C_2H_4+H]^+$, 325.1436 $[M+H]^+$, 347.1255 $[M+Na]^+$, 631.2710 $[2M\text{-}H_2O+H]^+$. RT: 8.80–8.90 min.

2. NMR spectroscopic data for **1–8**

Table S1. Spectroscopic values of deoxyenhygrolide C and D (**1** and **2**) acquired in $CDCl_3$ at 700 MHz.

Position	Deoxyenhygrolide C (**1**)				Deoxyenhygrolide D (**2**)			
	δ_C	**δ_H [m, *J* (Hz)]**	**HMBC**	**ROESY**	**δ_C**	**δ_H [m, *J* (Hz)]**	**HMBC**	**ROESY**
1	170.7,	-	-	-	170.1	-	-	-
2	126.1,	-	-	-	130.8	-	-	-
3	154.9	-	-	-	152.8	-	-	-
4	148.0	-	-	-	149.5	-	-	-
5	109.1	6.02, s	3, 4, (6), 7/11	19	114.7	6.86, s	3, 4, (6), 7/11	-
6	133.3	-	-	-	133.2	-	-	-
7/11	130.6	7.78, m	5, 7/11, 8/9/10	-	129.3	7.30, m	5	-
8/10	128.9	7.38, m	6, 7/11, 8/9/10	-	128.5	7.35, m	-	-
9	128.9	7.31, m	7/11	-	128.9	7.27, m	-	-
12	29.8	3.74, s	1, 2, 3, (4), 13, 14/18	-	29.7	3.69, s	1, 2, 3, (4), 13, 14/18	-
13	138.1	-	-	-	137.9	-	-	-
14/18	128.6	7.27, m	12	-	128.7	7.24, m	12	-
15/17	128.9	7.29, m	13	-	128.9	7.28, m	13	-
16	126.8	7.21, m	(13), 14/18	-	128.9	7.27, m	-	-
19	18.4	2.58, q, 7.7	2, 3, 4, 20	5	19.4	2.28, q, 7.6	2, 3, 4, 20	-
20	14.1	1.15, t, 7.7	3, 19	-	12.9	0.64, t, 7.6	3, 19	-

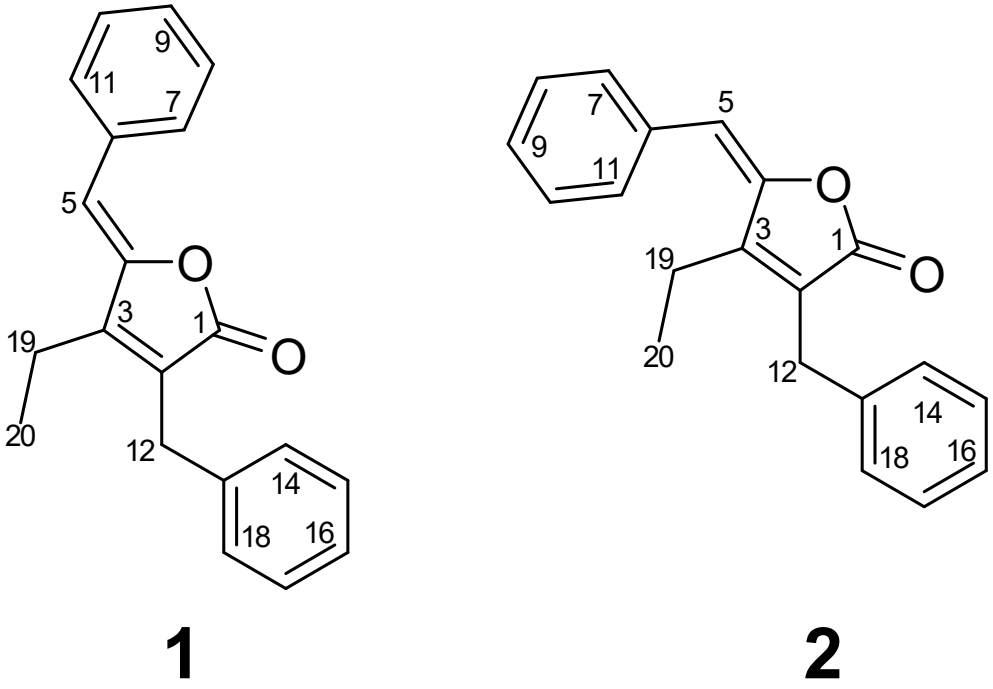

Figure S15. Structure and carbon numbering of deoxyenhygrolide C and D (**1** and **2**).

Table S2. Spectroscopic values of deoxyenhygrolide E and F (**3** and **4**) acquired in $CDCl_3$ at 500 MHz.

Position	Deoxyenhygrolide E (**3**)				Deoxyenhygrolide F (**4**)			
	δ_C	δ_H [m, *J* (Hz)]	HMBC	ROESY	δ_C	δ_H [m, *J* (Hz)]	HMBC	ROESY
1	166.9	-	-	-	166.2	-	-	-
2	124.2	-	-	-	129.4	-	-	-
3	164.7	-	-	-	161.2	-	-	-
4	147.1	-	-	-	148.8	-	-	-
5	113.9	6.36, s	(1), 3, 4, (6), 7/11	19	119.6	7.16, s	3, 4, (6), 7/11	-
6	132.6	-	-	-	132.4	-	-	-
7/11	131.4	7.88, m	5, 7/11	-	129.2	7.37, m	5, 6	19
8/10	129.2	7.45, m	6, 8/10	-	129.2	7.44, m	6, 8/10	-
9	130.1	7.41, m	-	-	128.8	7.41, m	-	-
12	190.0	-	-	-	190.2	-	-	-
13	136.7	-	-	-	136.4	-	-	-
14/18	129.7	7.88, m	12, 14/18, 16	-	129.7	7.87, m	12, 14/18, 16	-
15/17	128.8	7.50, m	13, 14/18, 15/17	-	128.8	7.50, m	13, 14/18, 15/17	-
16	134.2	7.63, m	14/18	-	134.4	7.63, m	14/18	-
19	19.2	2.78, q, 7.5	(1), 2, 3, 4, 20	5	20.3	2.40, q, 7.5	(1), 2, 3, 4, 20	7/11
20	15.0	1.32, t, 7.5	3, 19	-	13.6	0.80, t, 7.5	3, 19	-

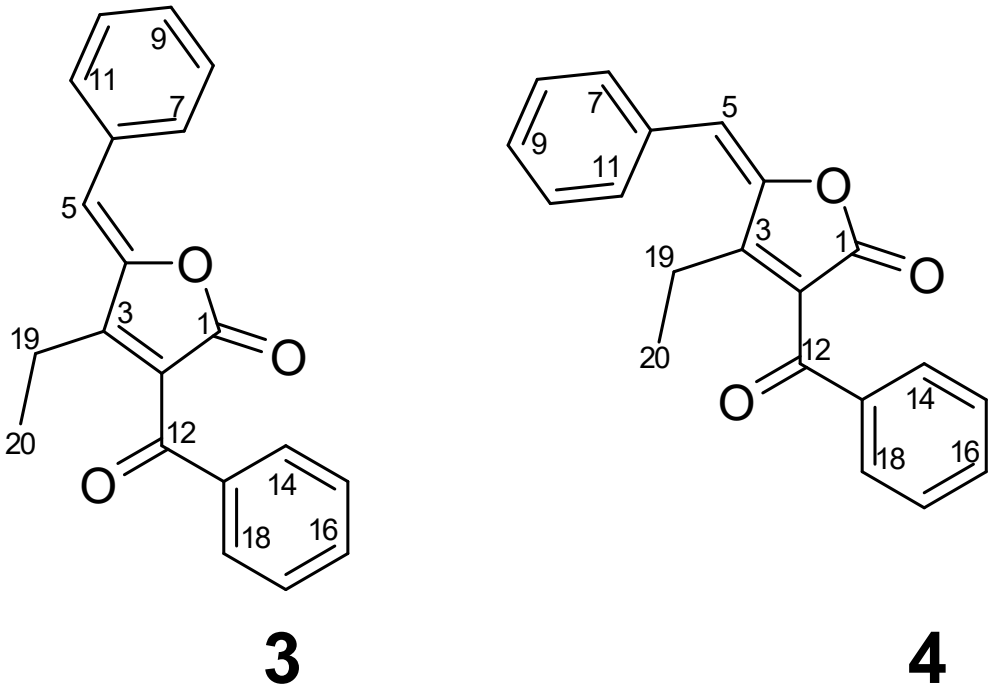

Figure S16. Structure and carbon numbering of deoxyenhygrolide E and F (**3** and **4**).

Table S3. Spectroscopic values of deoxyenhygrolide G and H (**5** and **6**) acquired in $CDCl_3$ at 700 MHz.

Position	Deoxyenhygrolide G (**5**)				Deoxyenhygrolide H (**6**)			
	δ_C	**δ_H [m, *J* (Hz)]**	**HMBC**	**ROESY**	**δ_C**	**δ_H [m, *J* (Hz)]**	**HMBC**	**ROESY**
1	169.9	-	-	-	169.4	-	-	-
2	126.9	-	-	-	131.2	-	-	-
3	155.1	-	-	-	152.8	-	-	-
4	147.4	-	-	-	149.0	-	-	-
5	110.8	6.11, s	(1), 3, 4, 7/11	7/11, 19	116.8	6.97, s	3, 4, (6), 7/11, (12)	-
6	132.9	-	-	-	132.7	-	-	-
7/11	130.8	7.78, m	5, 9, 7/11	5	129.2	7.31, m	5, 9, 8/10	-
8/10	129.0	7.39, m	6, 7/11 ,8/10	-	128.6	7.35–7.39, m	-	-
9	129.3	7.33, m	6, 7/11	-	128.8	7.35–7.39, m	-	-
12	68.9	5.78, br s	1, 2, 3, 13, 14/18	19	68.9	5.69, br s	1, 2, 3, 13, 14/18	19
12-OH	-	3.44, br s	(2)	-	-	3.64, br s	2, 12, (13)	-
13	141.5	-	-	-	141.5	-	-	-
14/18	126.1	7.46, m	12, 14/18, 16	-	126.2	7.42, m	12, 14/18, 16	-
15/17	128.9	7.37, m	13, (14/18), 15/17	-	128.9	7.36, m	13, (14/18), 15/17	-
16	128.2	7.30, m	(13), 14/18	-	128.3	7.30, m	14/18, 15/17	-
19	18.2	2.62, q, 7.7	(1), 2, 3, 4, 20	5, 12	19.2	2.32, q, 7.6	(1), 2, 3, 4, 20	12
20	14.4	1.17, t, 7.7	3, 19	-	13.0	0.67, t, 7.6	3, 19	-

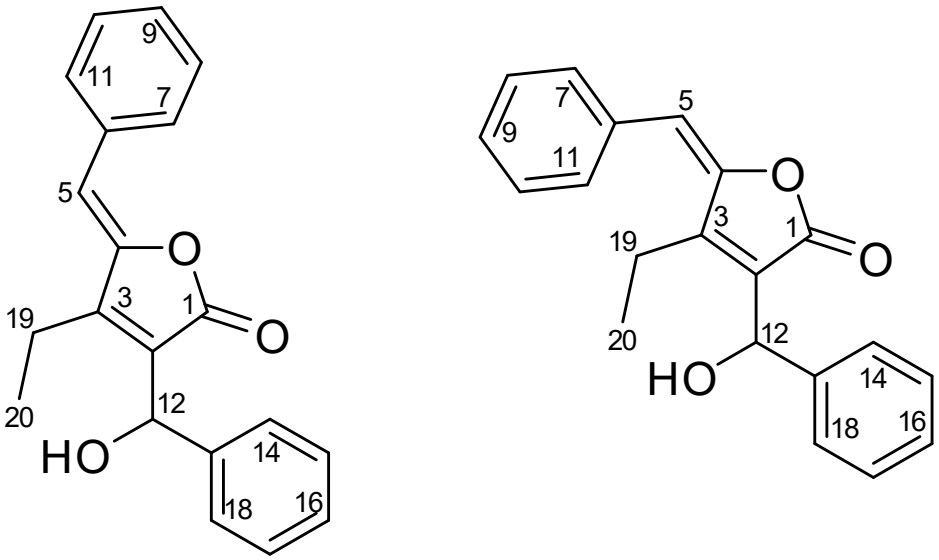

5 **6**

Figure S17. Structure and carbon numbering of deoxyenhygrolide G and H (**5** and **6**).

Table S4. Spectroscopic values of deoxyenhygrolide I and J (**7** and **8**) acquired in CD_3OD at 700/500 MHz, respectively.

Position	Deoxyenhygrolide I (**7**)			Deoxyenhygrolide J (**8**)		
	δ_C	**δ_H [m, *J* (Hz)]**	**HMBC**	**δ_C**	**δ_H [m, *J* (Hz)]**	**HMBC**
1	173.5	-	-	172.8	-	-
2	129.3	-	-	132.3	-	-
3	165.2	-	-	166.4	-	-
4	109.1	-	-	109.3	-	-
5	43.2	3.21, br s 3.35, br s	-	43.6	3.21, br s 3.33, br s	-
6	135.4	-	-	135.5	-	-
7/11	131.1	7.17, m	5, 9, 7/11	128.2	7.23, m	(5), 9, 8/10
8/10	129.0	7.20, m	6 ,8/10	129.4	7.20, m	6 ,8/10
9	127.9	7.23, m	7/11, (8/10)	131.4	7.15, m	-
12	29.3	3.42, br s	1, 2, 3, 13, 14/18	68.2	5.43, br s	1, 2, 3, 13, 14/18
13	138.5	-	-	142.7	-	-
14/18	128.8	6.65, m	12, (13), 14/18, 16	126.9	6.81, br s	-
15/17	129.1	7.09, m	13, 15/17	129.2	7.15, m	(12), 13, 15/17
16	126.8	7.09, m	-	128.1	7.15, m	14/18
19	20.6	2.42, q, 7.7	2, 3, 4, 20	20.8	2.48, q, 7.6	2, 3, 4, 20
20	12.1	1.17, t, 7.7	3, 19	13.4	1.22, t, 7.6	3, 19

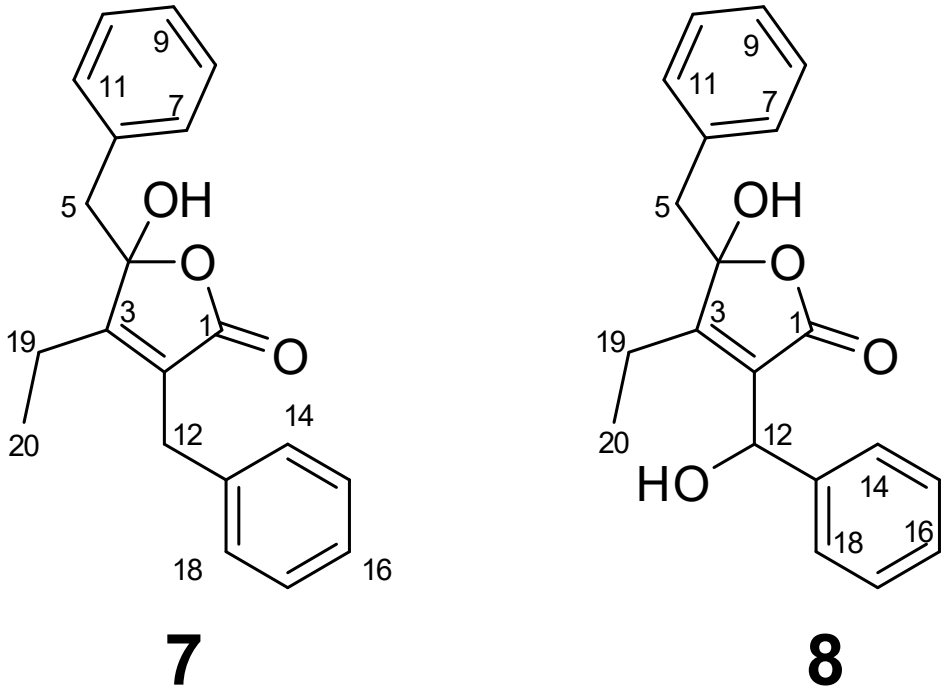

7 **8**

Figure S18. Structure and carbon numbering of deoxyenhygrolide I and J (**7** and **8**).

Table S5. Comparison of ^{13}C chemical shifts for **1–8**.

	1	2	3	4	5	6	7	8
Pos.	**$CDCl_3$**	**$CDCl_3$**	**$CDCl_3$**	**$CDCl_3$**	**$CDCl_3$**	**$CDCl_3$**	**CD_3OD**	**CD_3OD**
1	170.7	170.1	166.9	166.2	169.9	169.4	173.5	172.8
2	126.1	130.8	124.2	129.4	126.9	131.2	129.3	132.3
3	154.9	152.8	164.7	161.2	155.1	152.8	165.2	166.4
4	148.0	149.5	147.1	148.8	147.4	149.0	109.1	109.3
5	109.1	114.7	113.9	119.6	110.8	116.8	43.2	43.6
6	133.3	133.2	132.6	132.4	132.9	132.7	135.4	135.5
7/11	130.6	129.3	131.4	129.2	130.8	129.2	131.1	128.2
8/10	128.9	128.5	129.2	129.2	129.0	128.6	129.0	129.4
9	128.9	128.9	130.1	128.8	129.3	128.8	127.9	131.4
12	29.8	29.7	190.0	190.2	68.9	68.9	29.3	68.2
13	138.1	137.9	136.7	136.4	141.5	141.5	138.5	142.7
14/18	128.6	128.7	129.7	129.7	126.1	126.2	128.8	126.9
15/17	128.9	128.9	128.8	128.8	128.9	128.9	129.1	129.2
16	126.8	128.9	134.2	134.4	128.2	128.3	126.8	128.1
19	18.4	19.4	19.2	20.3	18.2	19.2	20.6	20.8
20	14.1	12.9	15.0	13.6	14.4	13.0	12.1	13.4

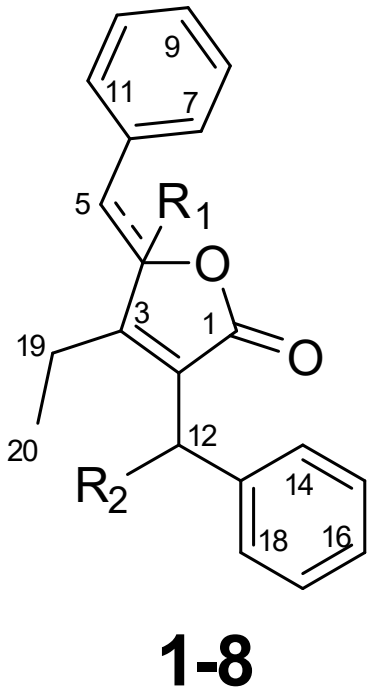

1-8

Figure S19. General structure and carbon numbering of deoxyenhygrolide A–H (**1–8**). (**1**) R1: –H, R2: –H, (*Z*); (**2**) R1: –H, R2: –H, (*E*); (**3**) R1: –H, R2: =O, (*Z*); (**4**) R1: –H, R2: =O, (*E*); (**5**) R1: –H, R2: –OH, (*E*); (**6**) R1: –H, R2: –OH, (*Z*); (**7**) R1: –OH, R2: –H; (**8**) R1: –OH, R2: –OH.

3. Genetic and biosynthetic investigations

3.1 Identification of *cybE* and *cybF* homologs in different myxobacteria

The myxobacterial gene homologs of *cybE* and *cybF* were identified in *Enhygromyxa salina* SWB005 (GenBank accession number: PVNK00000000.1) on contig000249 (GenBank accession number: PVNK01000249.1), in *Enhygromyxa salina* SWB007 (GenBank accession number: PVNL00000000.1) on contig000074 (GenBank accession number: PVNL01000074.1) and in *Plesiocystis pacifica* DSM 14875^T (GenBank accession number: ABCS00000000.1) on contig1000004 (GenBank accession number: ABCS01000004.1). Interestingly, between the co-localized gene homologs *cybE* and *cybF* in *E. salina* SWB007 (not in *E. salina* SWB005), an open reading frame (ORF) is located, which is putatively encoding a homolog of a flavin-dependent tryptophan halogenase (PrnA) which was described in the biosynthesis of pyrrolnitrin [1]. The size in base pairs (bp) and locus tag of the respective *cybE* or *cybF* are given in **Table S6**.

Table S6. *cybE* and *cybF* homologs identified in different myxobacterial genome sequences.

	cybE		***cybF***	
Organism	**Locus Tag**	**Size [bp]**	**Locus Tag**	**Size [bp]**
Tolypothrix sp. PCC 9009	*Tol9009DRAFT_00039900*	1872	*Tol9009DRAFT_00039890*	1131
Plesiocystis pacifica DSM 14875^T	PPSIR1_40640	1536	PPSIR1_40635	1107
Enhygromyxa salina SWB005	ENSA5_56740	1674	ENSA5_56750	1113
Enhygromyxa salina SWB007	151239–152885(1)	1647	ENSA7_38410	1125

(1) No gene annotation available; interval of open reading frame is provided

Since the gene annotation in the publicly available myxobacterial genome sequence display shorter *cybE* homologs (1536/1674 bp vs. 1872 bp) or no gene annotation at all (SWB007), we further investigated the genome sequence of *P. pacifica* DSM 14875^T for the presence of a longer open reading frame and annotated the *cybE* homolog accordingly. The slightly different annotation is presented in **Table S7** alongside the pairwise sequence identity and positive percentage using BLSM62 substitution-scoring matrix [2] obtained by a pairwise alignment with *CybE* from *Tolypothrix sp.* PCC 9009.

Table S7. Changed locus tag of *cybE* homolog.

Organism	**Locus Tag**	**Size [bp]**	**Identity**	**Similarity**
Tolypothrix sp. PCC 9009	*Tol9009DRAFT_00039900*	1872	---	---
P. pacifica DSM 14875^T	134868–136562	1695	44.0%	61.6%
E. salina SWB005	ENSA5_56740	1674	43.3%	60.8%
E. salina SWB007	151239–152885(1)	1647	44.2%	61.8%

(1) (No) gene annotation available; interval of open reading frame is provided

Amino acid sequence alignment of the CybE/F homolog from *P. pacifica* DSM 14875^T (see **3.2**) show comparatively low but significant similarity to the *in vitro* investigated thiamine pyrophosphate (TPP)-binding protein CybE from *Tolypothrix* sp. PCC 9009 [3]. In addition to support the assigned function of the identified CybE homolog from *P. pacifica* DSM 14875^T, both CybE sequences were evaluated by *in silico* protein homology analogy recognition engine 2 (Phyre2), and the results indeed underline the structural similarity of both CybE enzymes to a structurally characterized flavin-dependent pyruvate oxidase from *Escherichia coli* (*Ec*POX, PDB: 3EY9) [4]. In contrast, Phyre2 analysis of both CybF enyzmes led to slightly different homology models; the CybE homolog from *P. pacifica* DSM 14875^T displays *in silico* structural similarity to a 3-Ketoacyl-ACP synthase **(**KAS III) from *Propionibacterium acnes* (PDB: 6A9N, [5]), whereas CybE from *Tolypothrix* sp. PCC 9009 seems structurally closer related to KAS III from *Vibrio cholerae* (PDB: 4X0O, [6]).

3.2 Sequence alignments and Phyre2 structures.

CybE

Figure S20. Amino acid alignment of myxobacterial CybE homologs from *P. pacifica* DSM 14875^T (CybE_Pacifica), *E. salina* SWB005 (CybE_SWB005) and *E. salina* SWB007 (CybE_SWB007). Pairwise identity: 45.0%, pairwise positive (BLSM62): 61.2%.

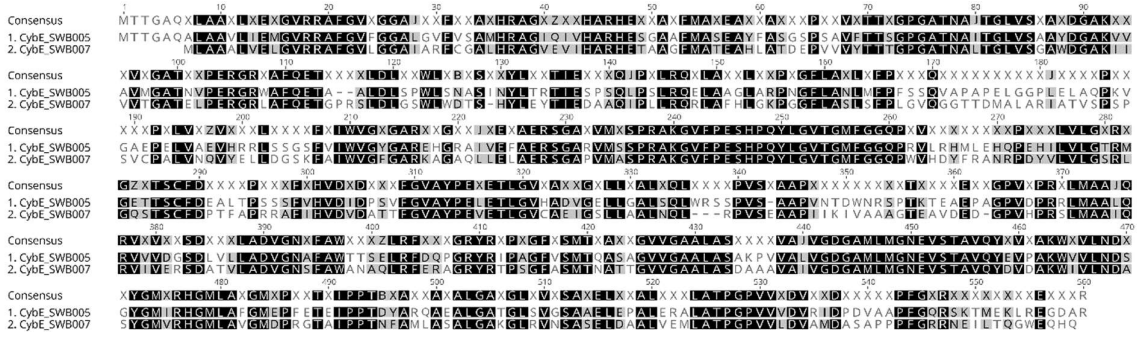

Figure S21. Amino acid alignment of myxobacterial CybE homologs from *E. salina* SWB005 (CybE_SWB005) and *E. salina* SWB007 (CybE_SWB007). Pairwise identity: 57.3%, pairwise positive (BLSM62): 72.3%.

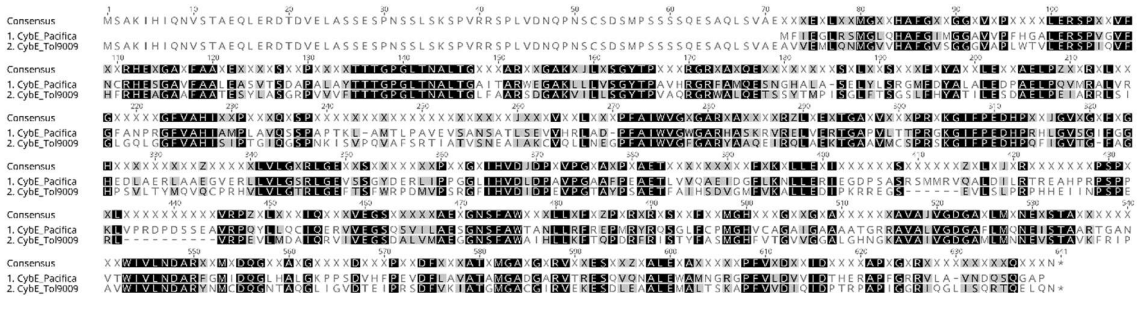

Figure S22. Amino acid alignment of myxobacterial CybE homolog from from *P. pacifica* DSM 14875^T (CybE_Pacifica) and CybE from *Tolypothrix sp.* PCC 9009 (CybE_Tol9009). Pairwise identity: 44.0%, pairwise positive (BLSM62): 61.6%.

CybF

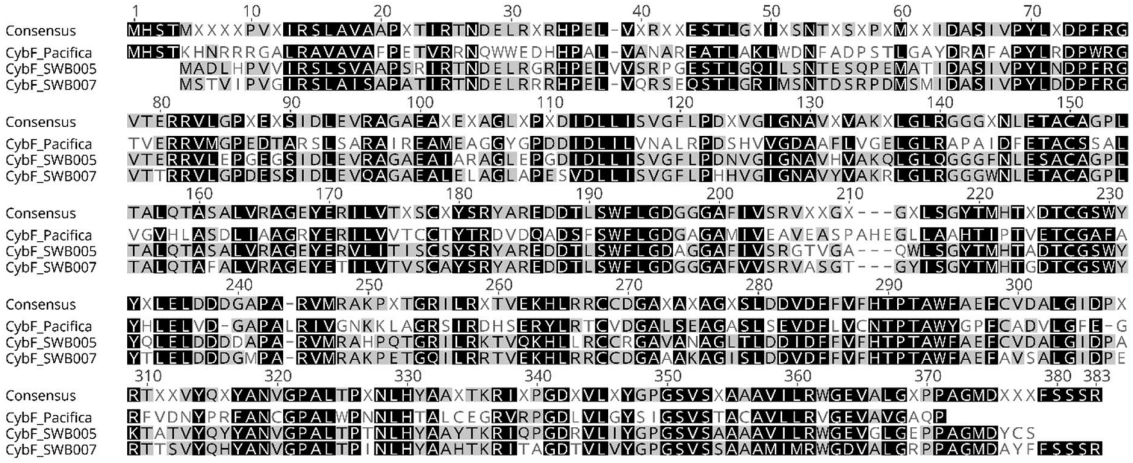

Figure S23. Amino acid alignment of myxobacterial CybF homologs from *P. pacifica* DSM 14875^T (CybF_Pacifica), *E. salina* SWB005 (CybF_SWB005) and *E. salina* SWB007 (CybF_SWB007). Pairwise identity: 50.8%, pairwise positive (BLSM62): 66.5%.

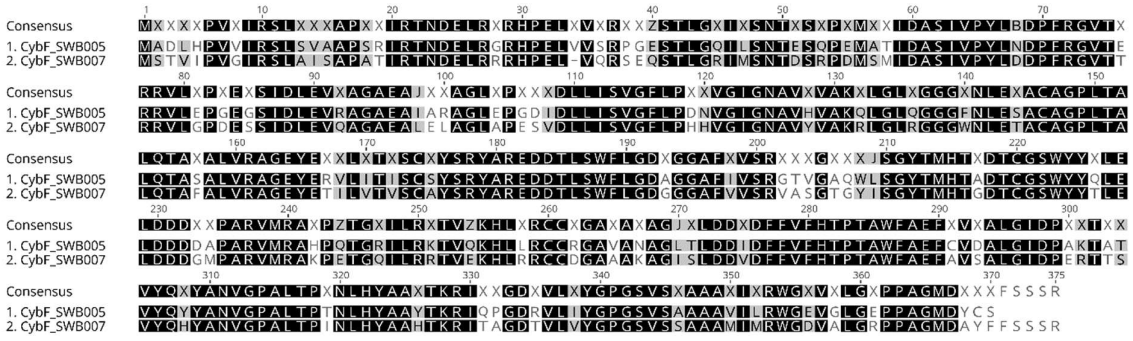

Figure S24. Amino acid alignment of myxobacterial CybF homologs from *E. salina* SWB005 (CybF_SWB005) and *E. salina* SWB007 (CybF_SWB007). Pairwise identity: 74.1%, pairwise positive (BLSM62): 86.5%.

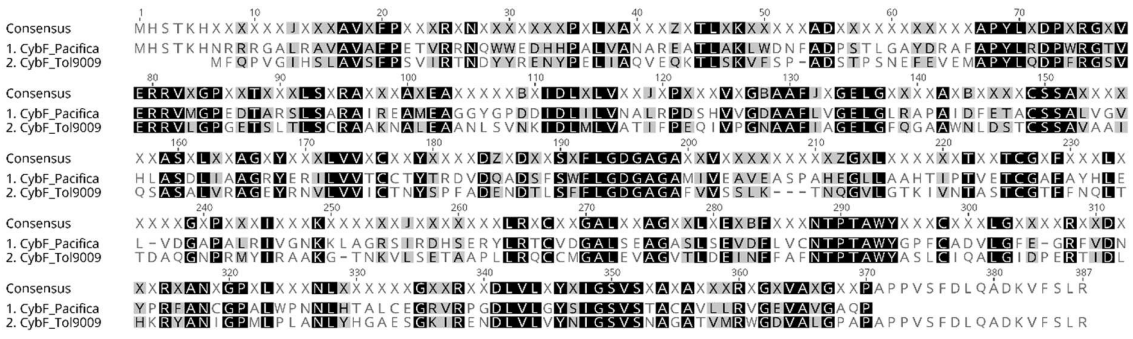

Figure S25. Amino acid alignment of myxobacterial CybF homolog from from *P. pacifica* DSM 14875^T (CybF_Pacifica) and CybF from *Tolypothrix sp.* PCC 9009 (CybE_Tol9009). Pairwise identity: 39.3%, pairwise positive (BLSM62): 59.6%.

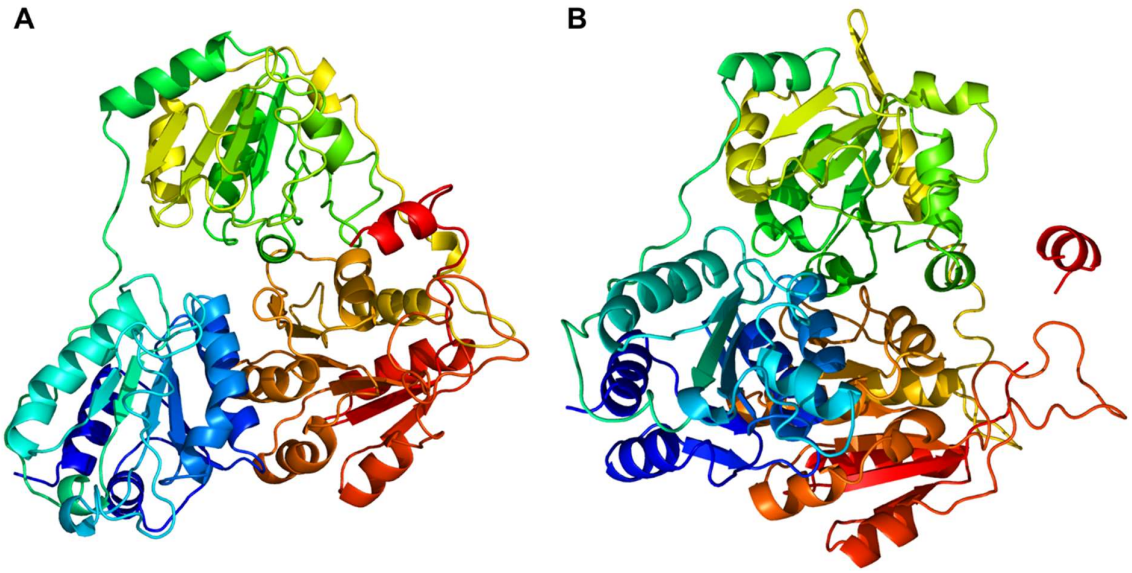

Figure S26. Phyre2 structure homology model of the thiamine pyrophosphate-binding protein (TPP) encoded by *cybE* from *Tolypothrix sp.* PCC 9009 (**A**) and the identified *cybE* homolog from *P. pacifica* DSM 14875^{T} (models are based on the template c3ey9B; figure colored by rainbow *N* → *C* terminus).

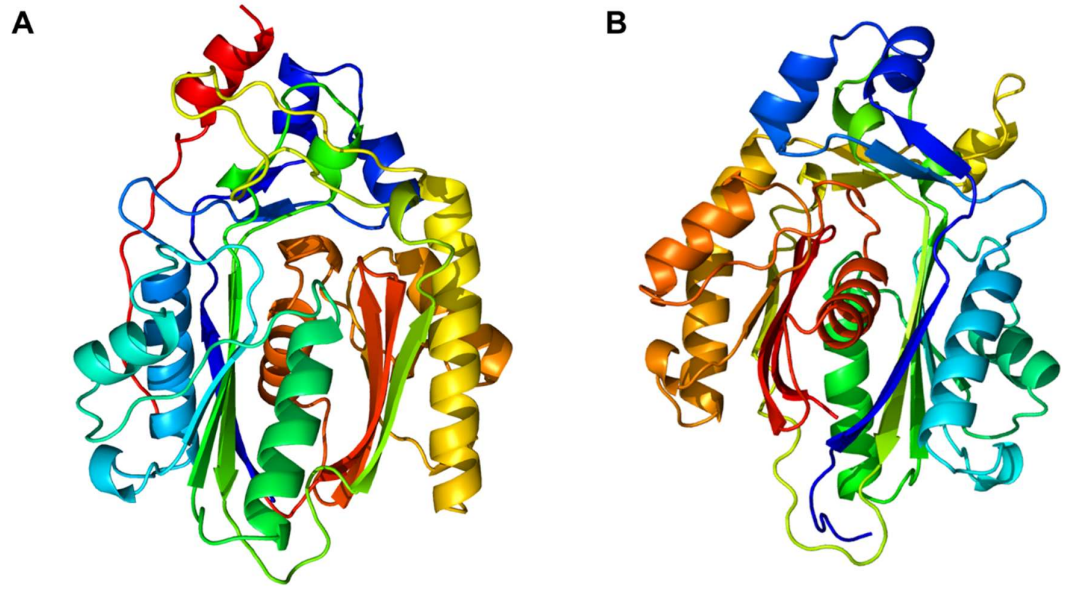

Figure S27. Phyre2 structure homology model of the furanolide encoded by *cybF* from *Tolypothrix sp.* PCC 9009 (**A**) and the identified *cybF* homolog from *Plesiocystis pacifica* DSM 14875^{T}. **A**) Model based on template c4x0oG. **B**) Model based on template c6a9nA; figure colored by rainbow *N* → *C* terminus).

4. ^{1}H and ^{13}C NMR spectra for **1–8**

4.1 NMR spectra of **1** and **2**

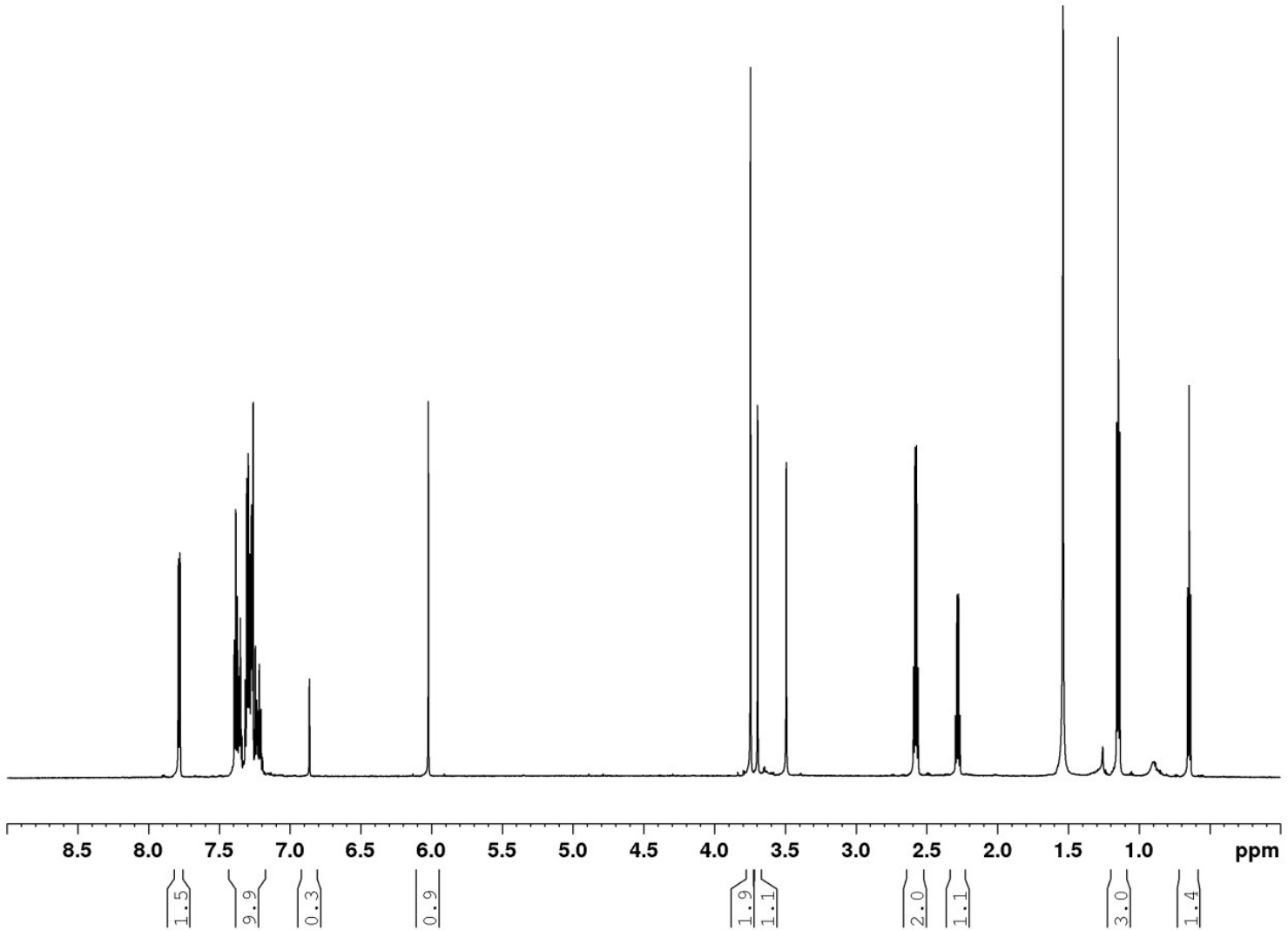

Figure S28. ^{1}H NMR spectrum of **1** and **2** (700 MHz, $CDCl_3$).

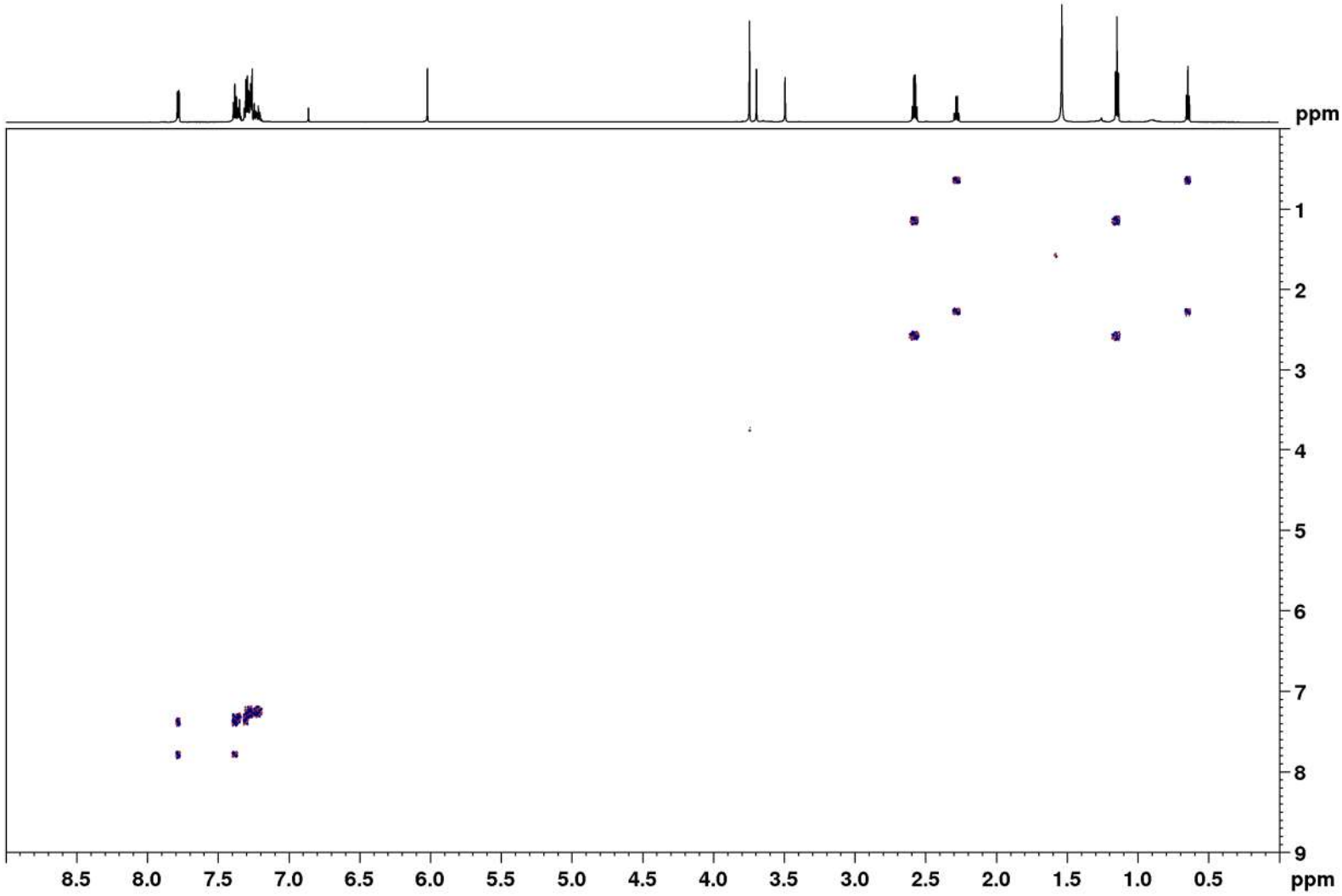

Figure S29. DQF-COSY spectrum of **1** and **2** (700 MHz, $CDCl_3$).

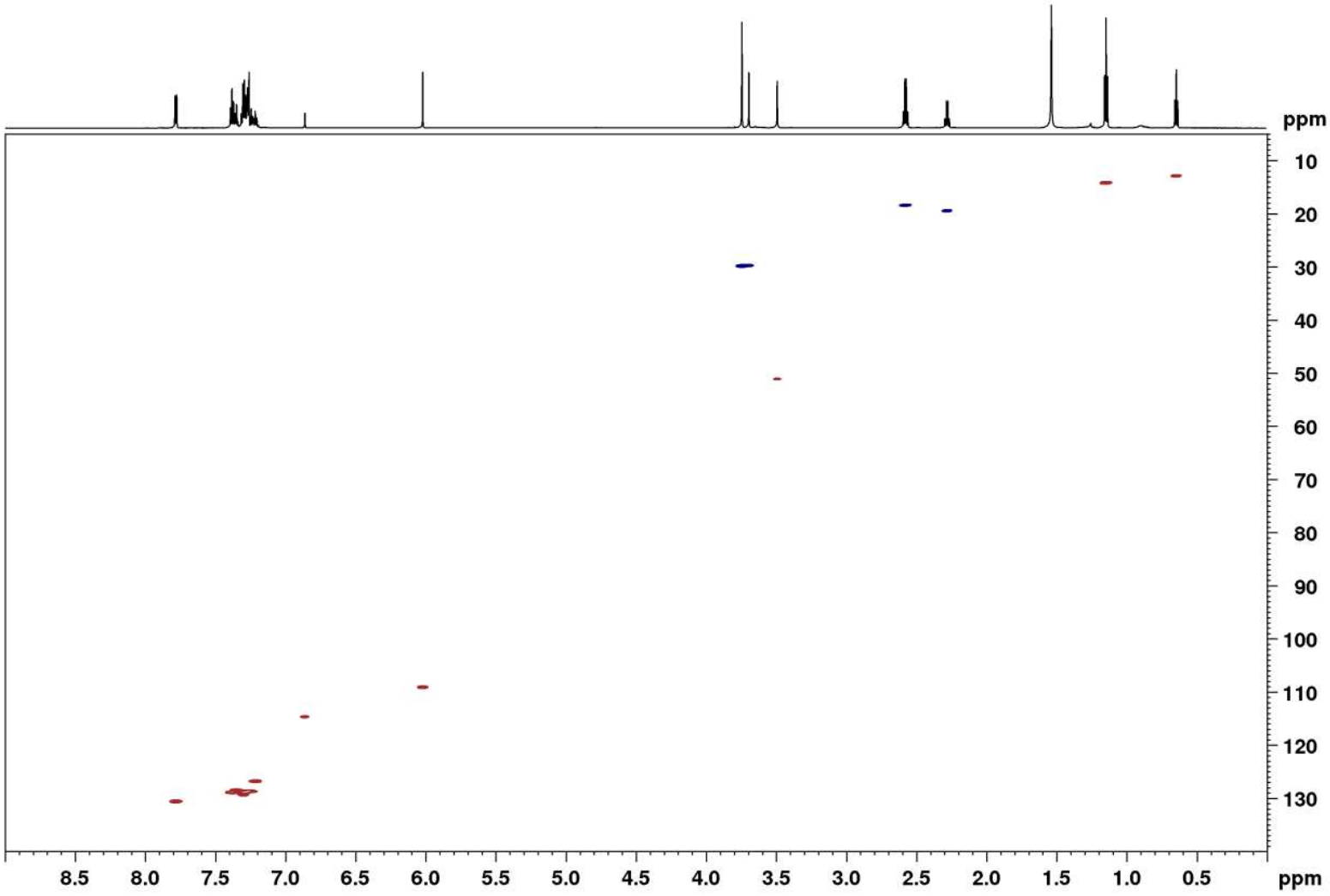

Figure S30. HSQC spectrum of **1** and **2** (700 MHz, $CDCl_3$).

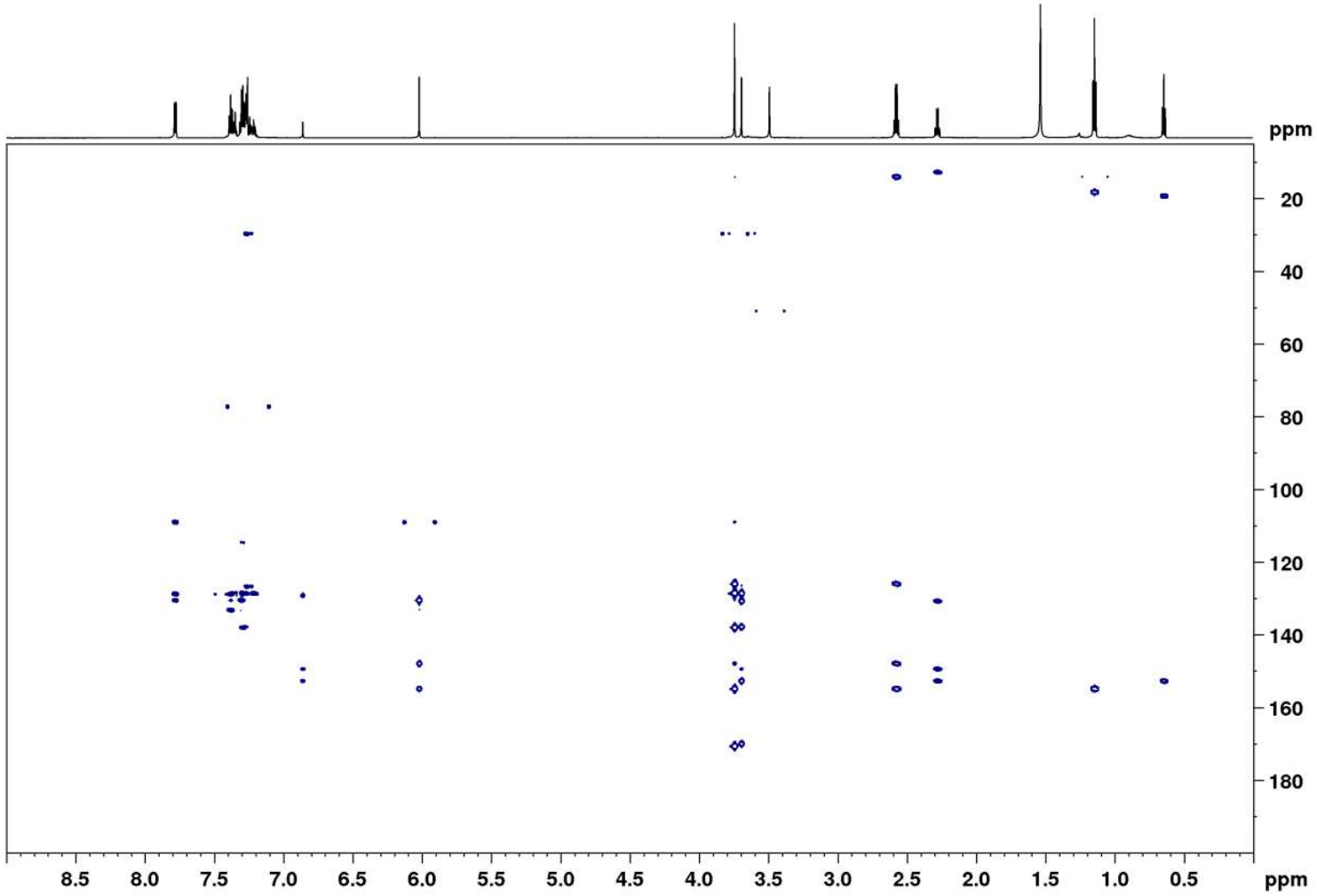

Figure S31. HMBC spectrum of **1** and **2** (700 MHz, $CDCl_3$).

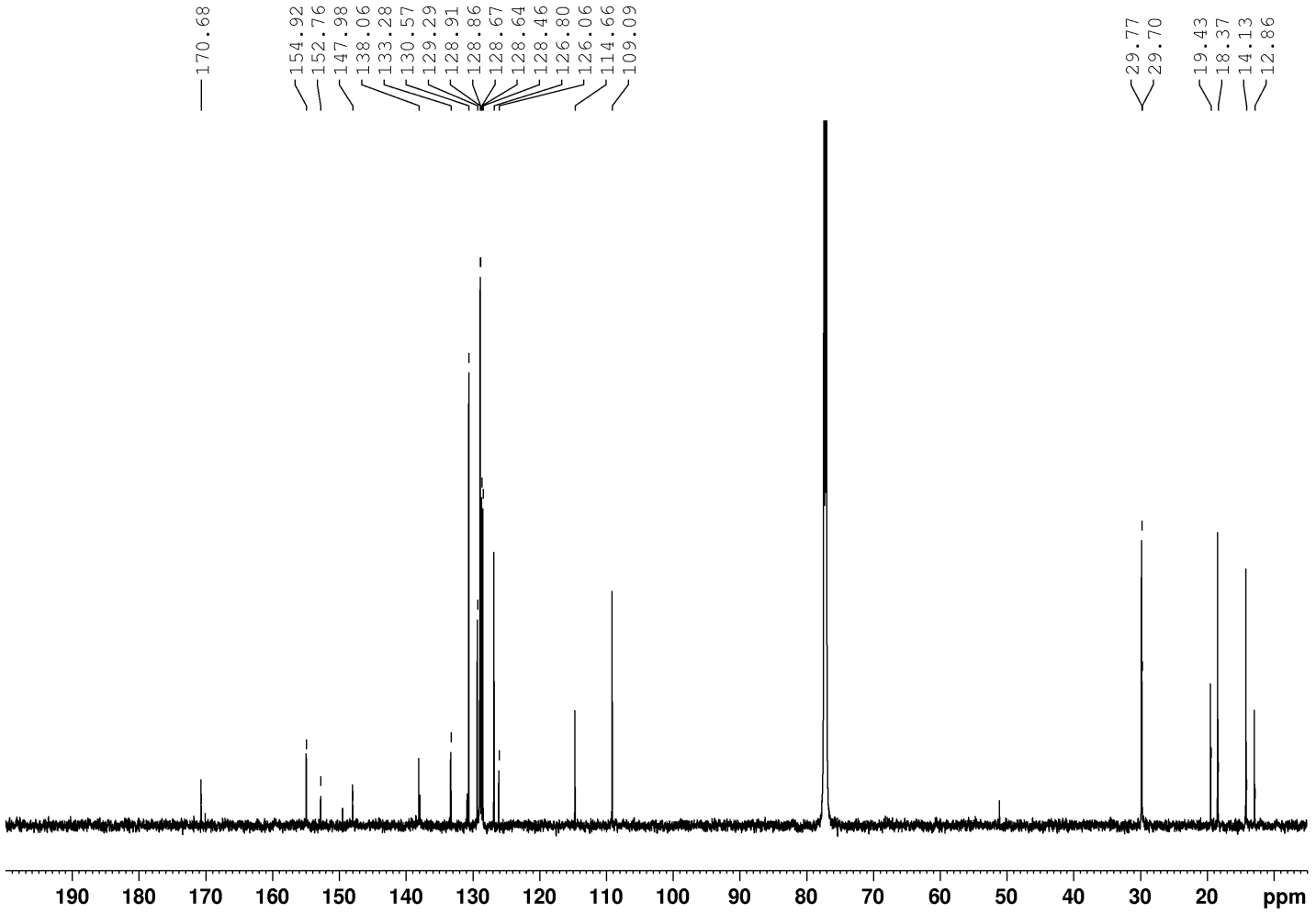

Figure S32. ^{13}C NMR spectrum of **1** and **2** (700 MHz, $CDCl_3$).

4.2 NMR spectra of **3** and **4**

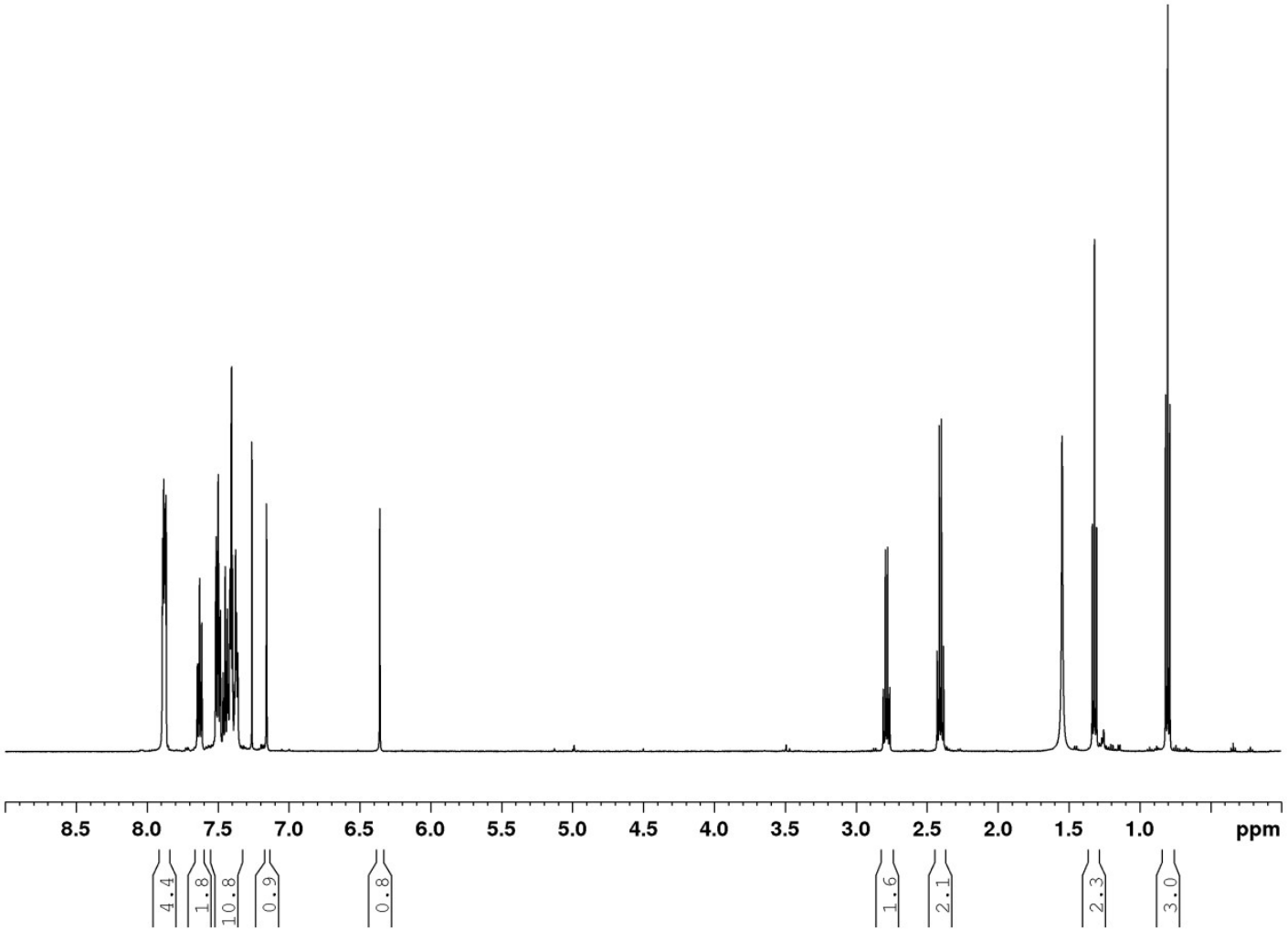

Figure S33. ^{1}H NMR spectrum of **3** and **4** (500 MHz, $CDCl_3$).

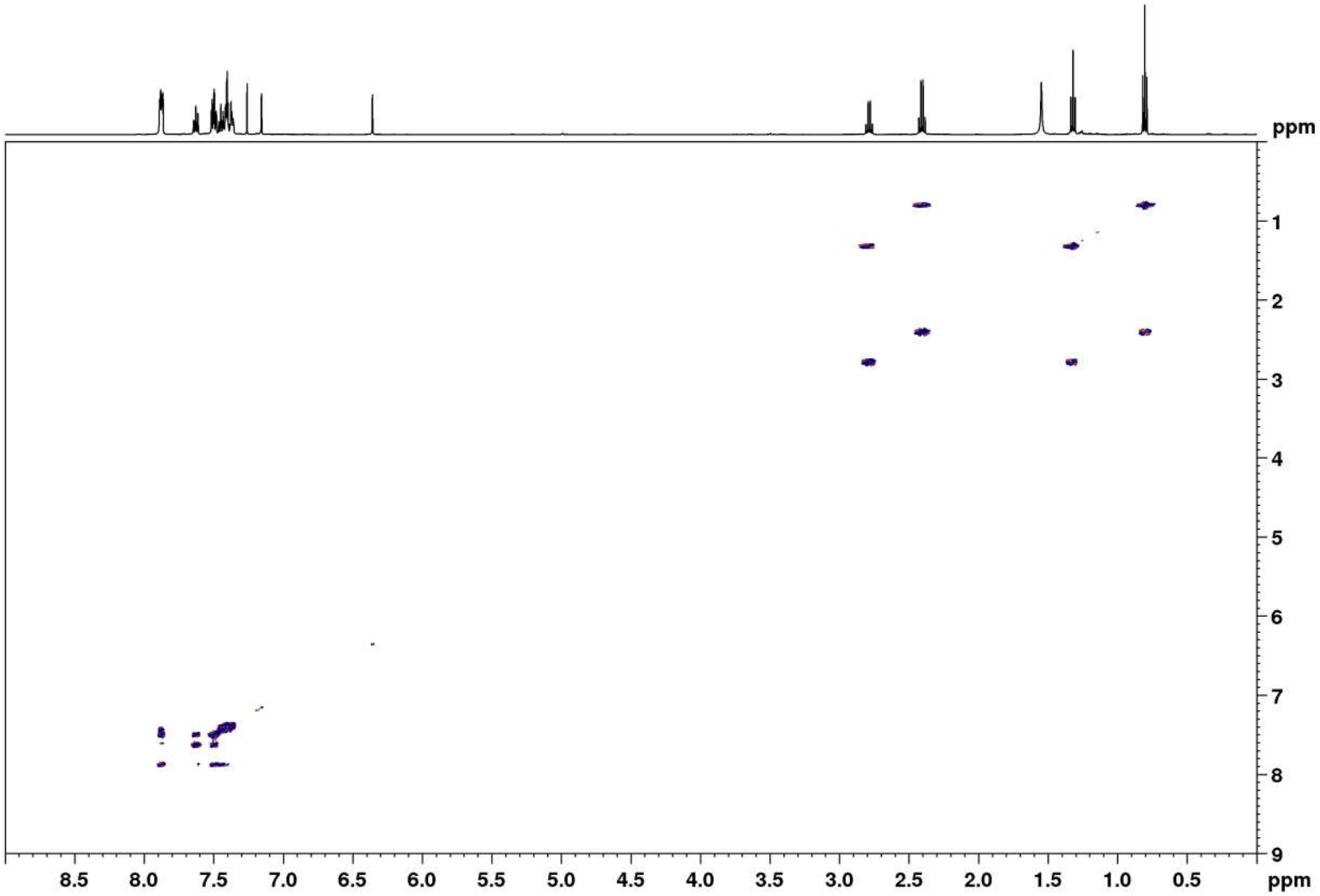

Figure S34. DQF-COSY spectrum of **3** and **4** (500 MHz, $CDCl_3$).

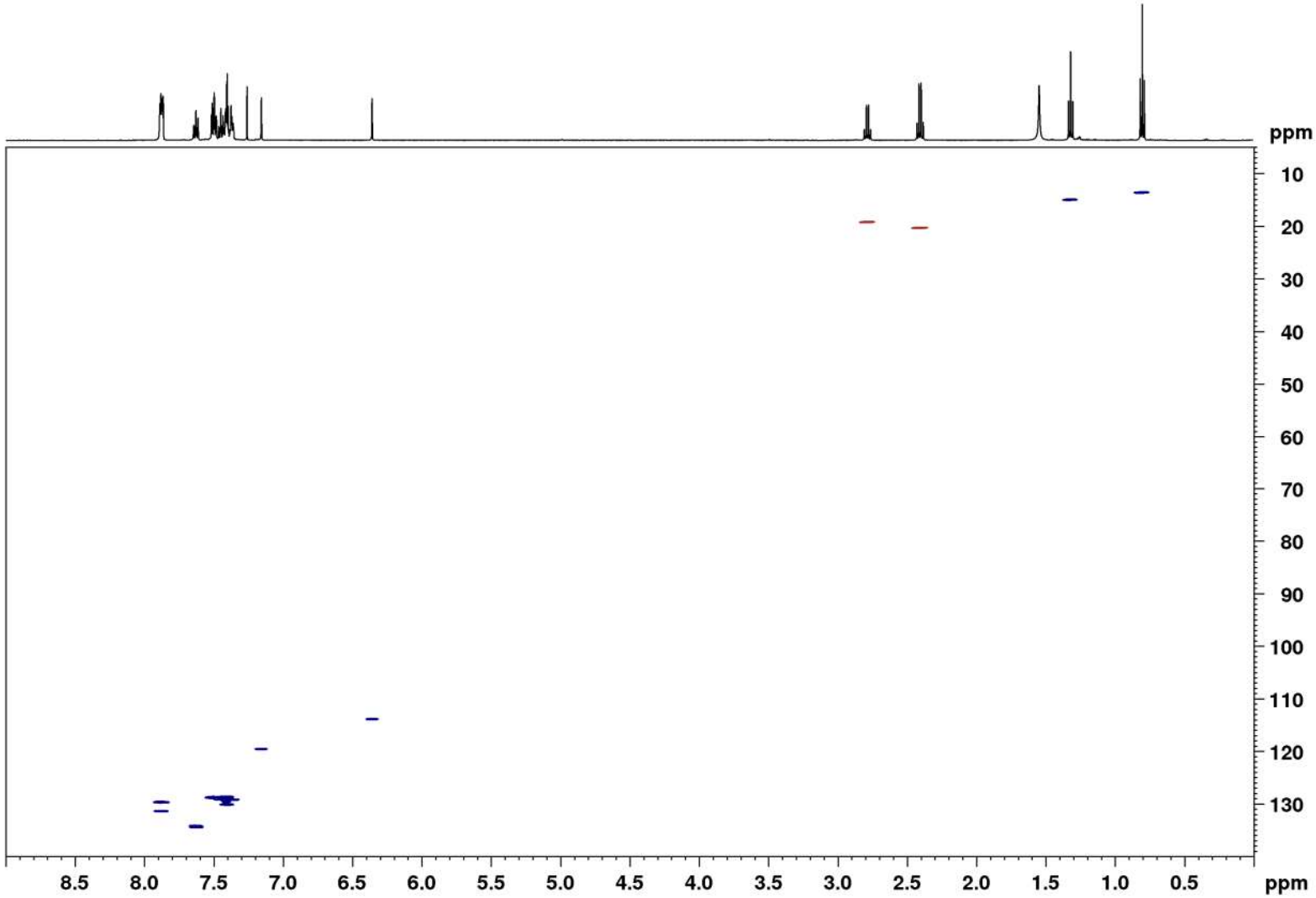

Figure S35. HSQC spectrum of **3** and **4** (500 MHz, $CDCl_3$).

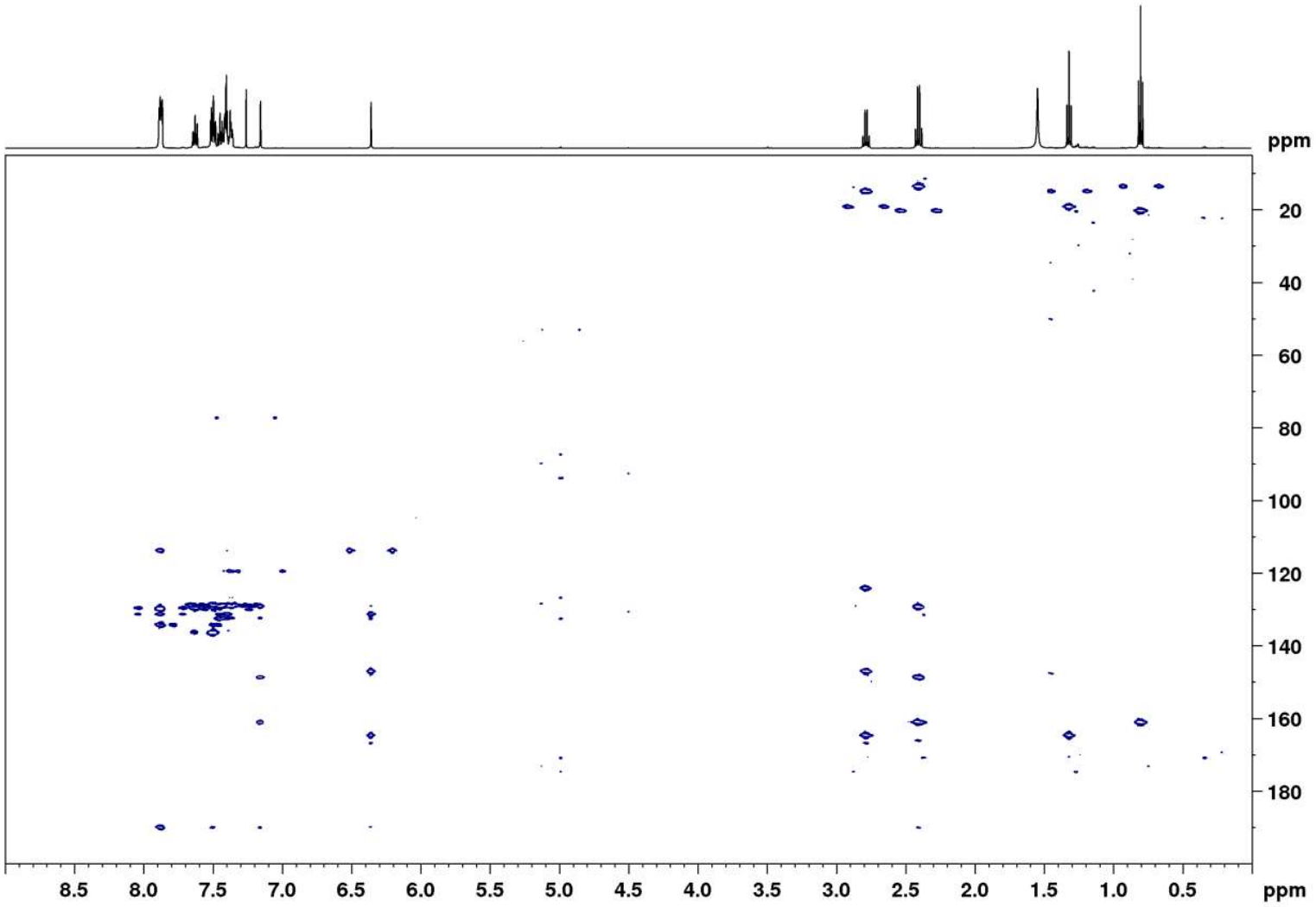

Figure S36. HMBC spectrum of **3** and **4** (500 MHz, $CDCl_3$).

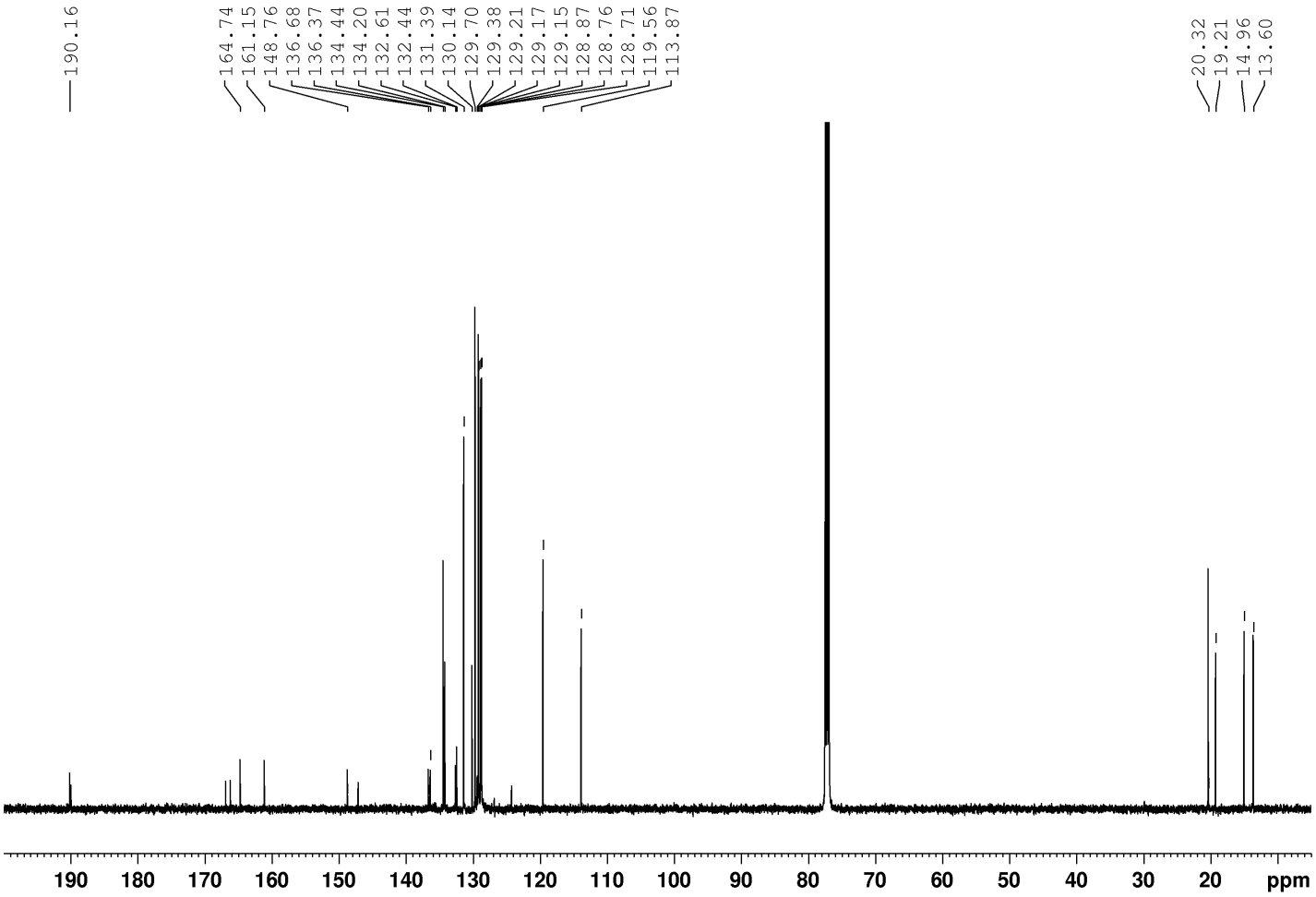

Figure S37. ^{13}C NMR spectrum of **3** and **4** (125 MHz, $CDCl_3$).

4.3 NMR spectra of **5**

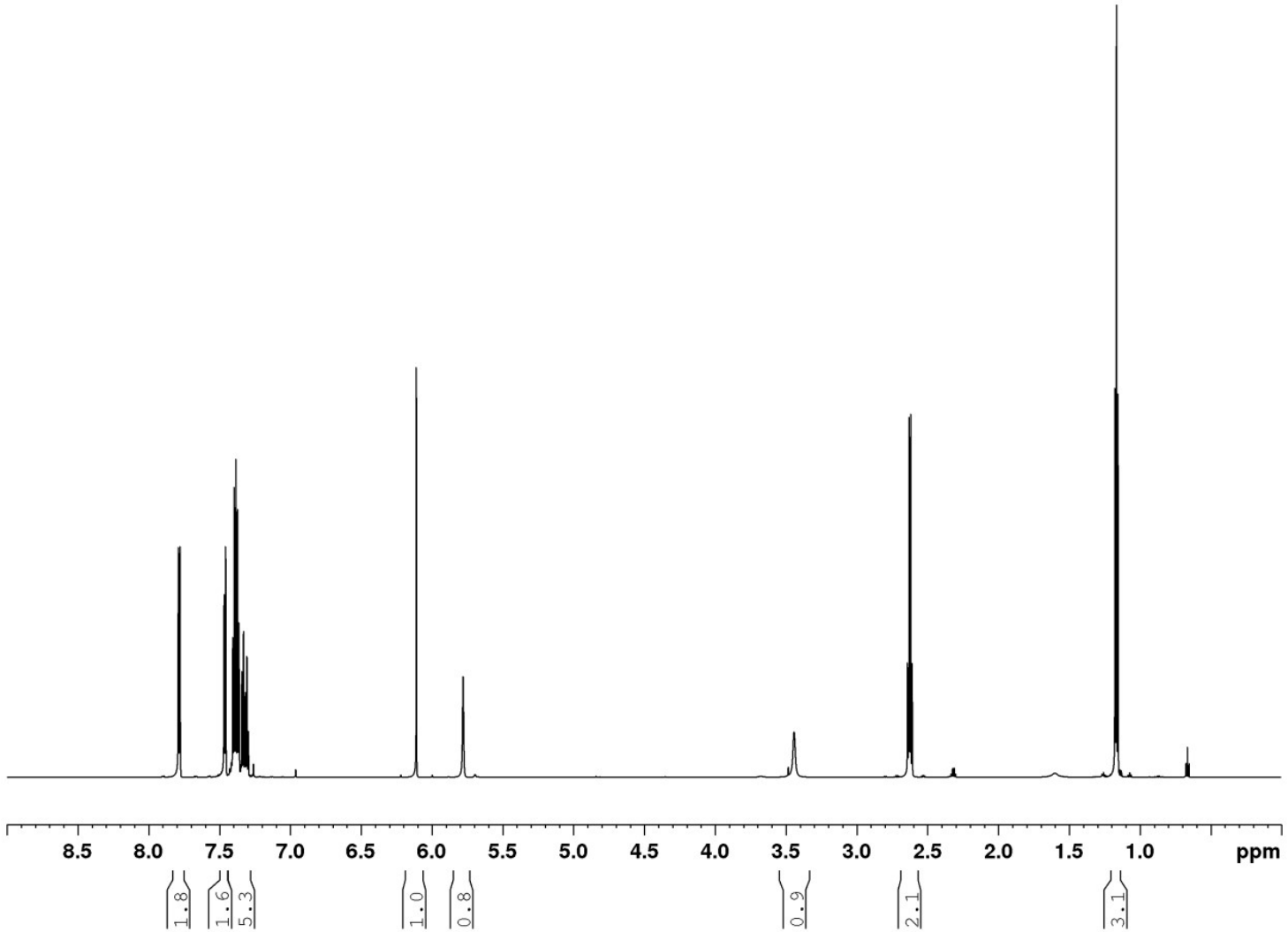

Figure S38. ^{1}H NMR spectrum of **5** (700 MHz, $CDCl_3$).

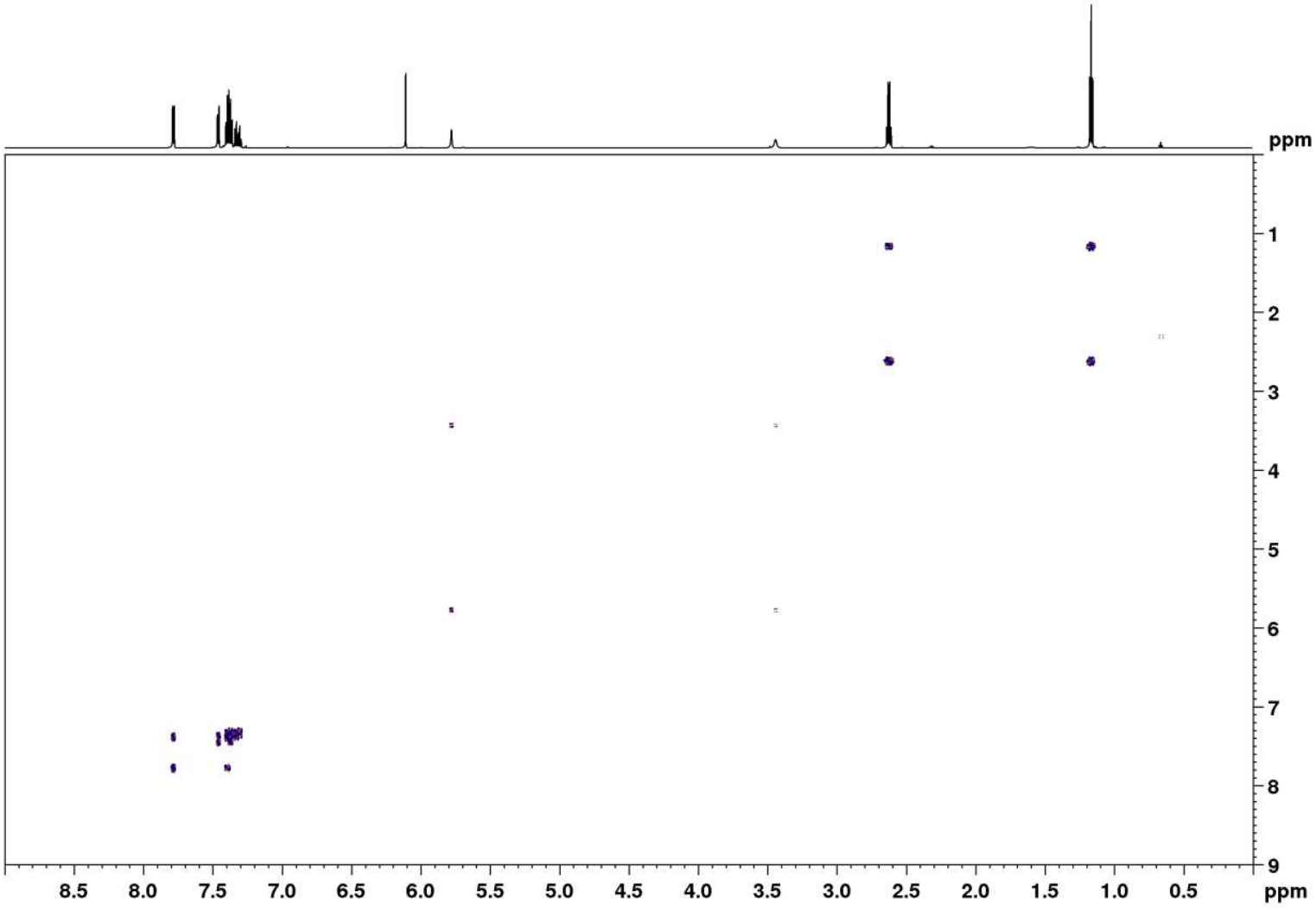

Figure S39. DQF-COSY spectrum of **5** (700 MHz, $CDCl_3$).

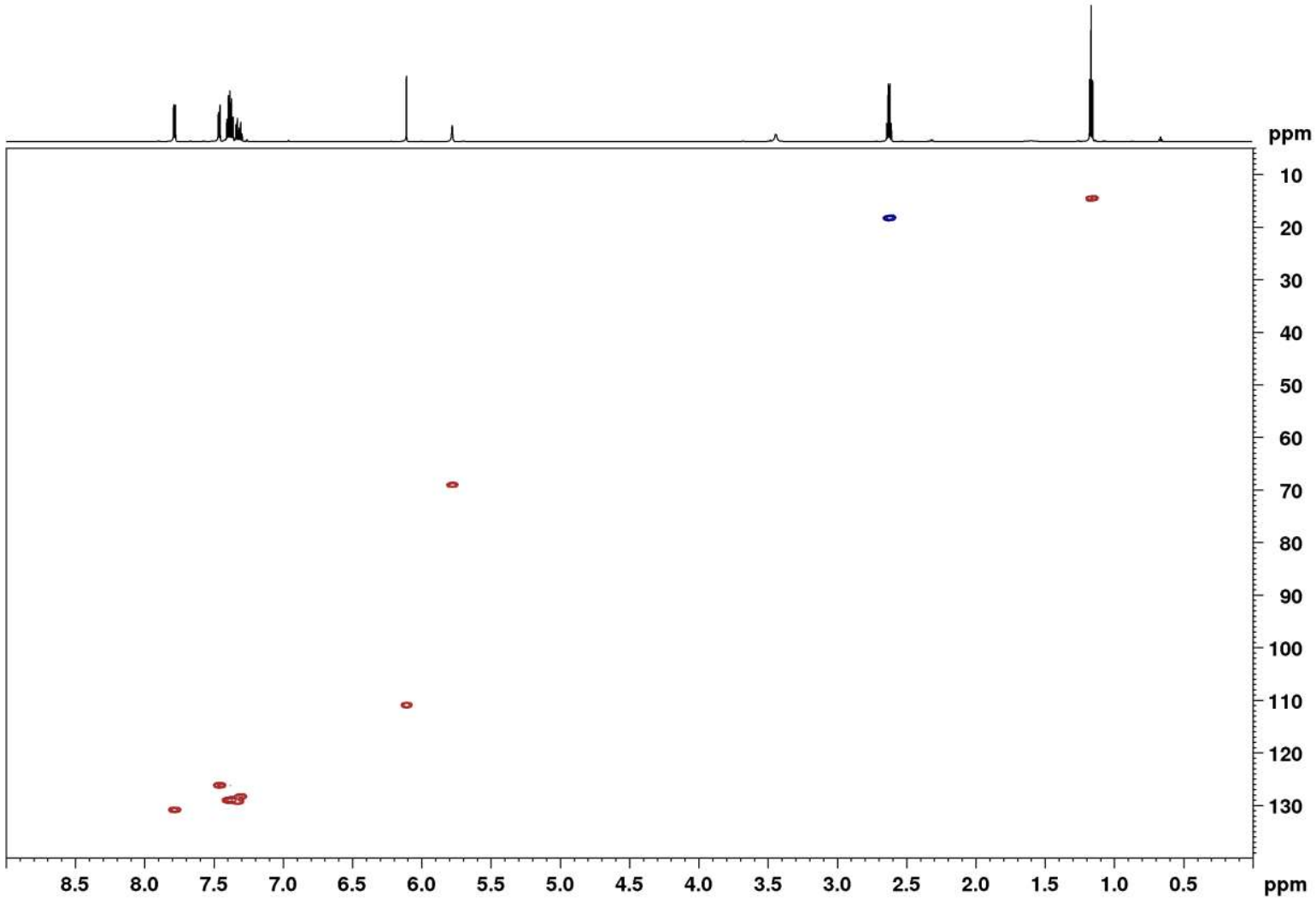

Figure S40. HSQC spectrum of **5** (700 MHz, $CDCl_3$).

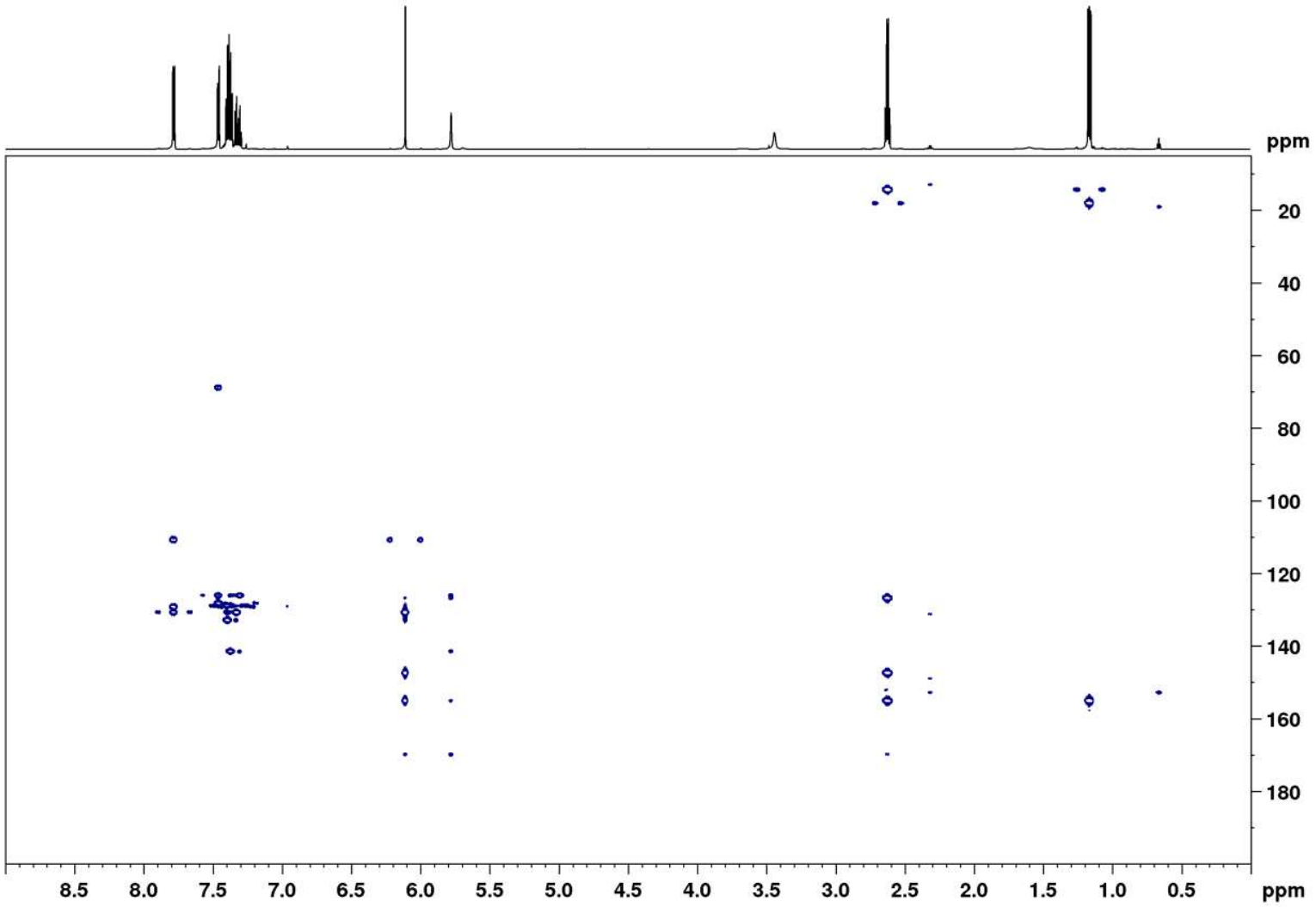

Figure S41. HMBC spectrum of **5** (700 MHz, $CDCl_3$).

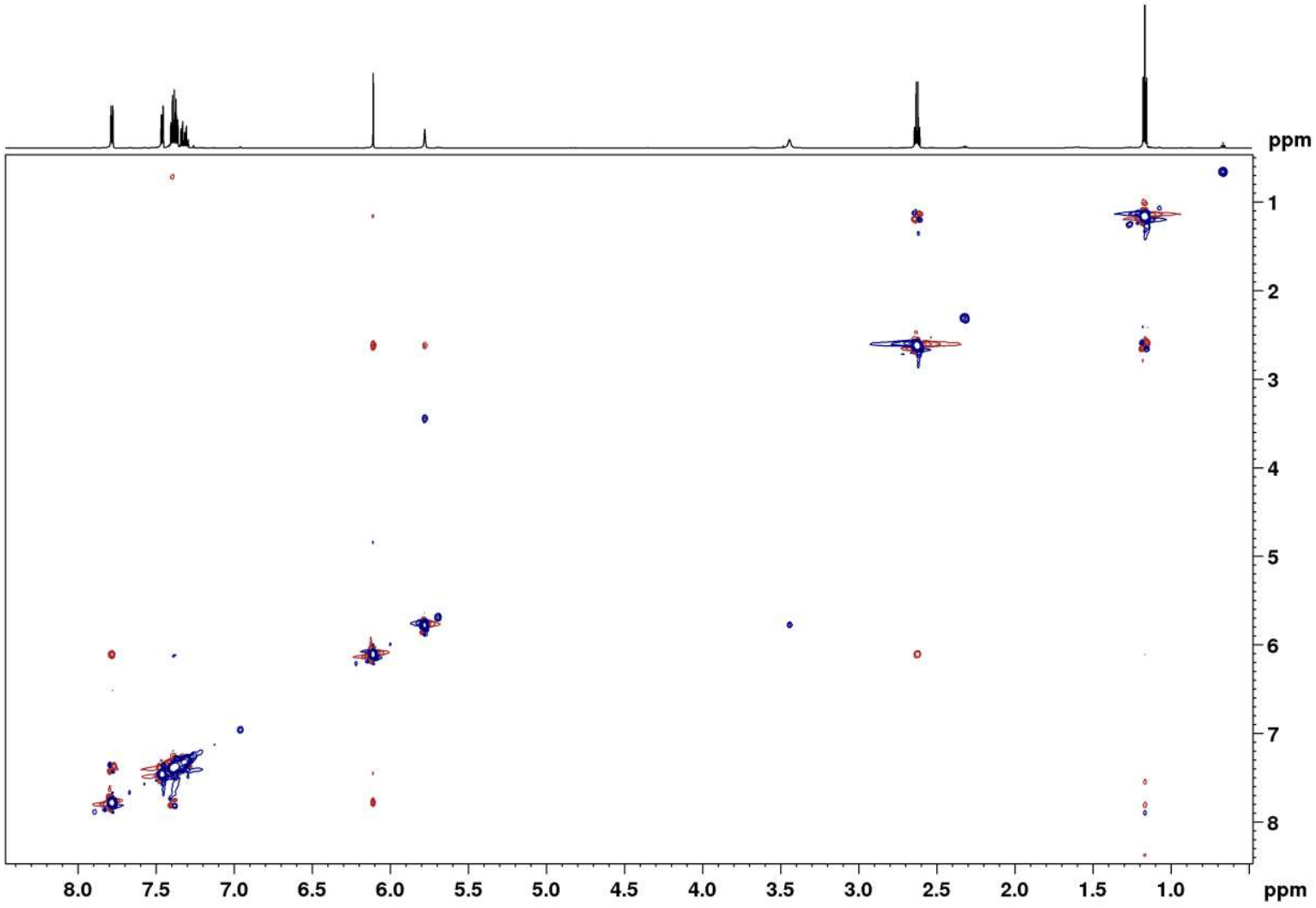

Figure S42. ROESY spectrum of **5** (700 MHz, $CDCl_3$, 400 ms).

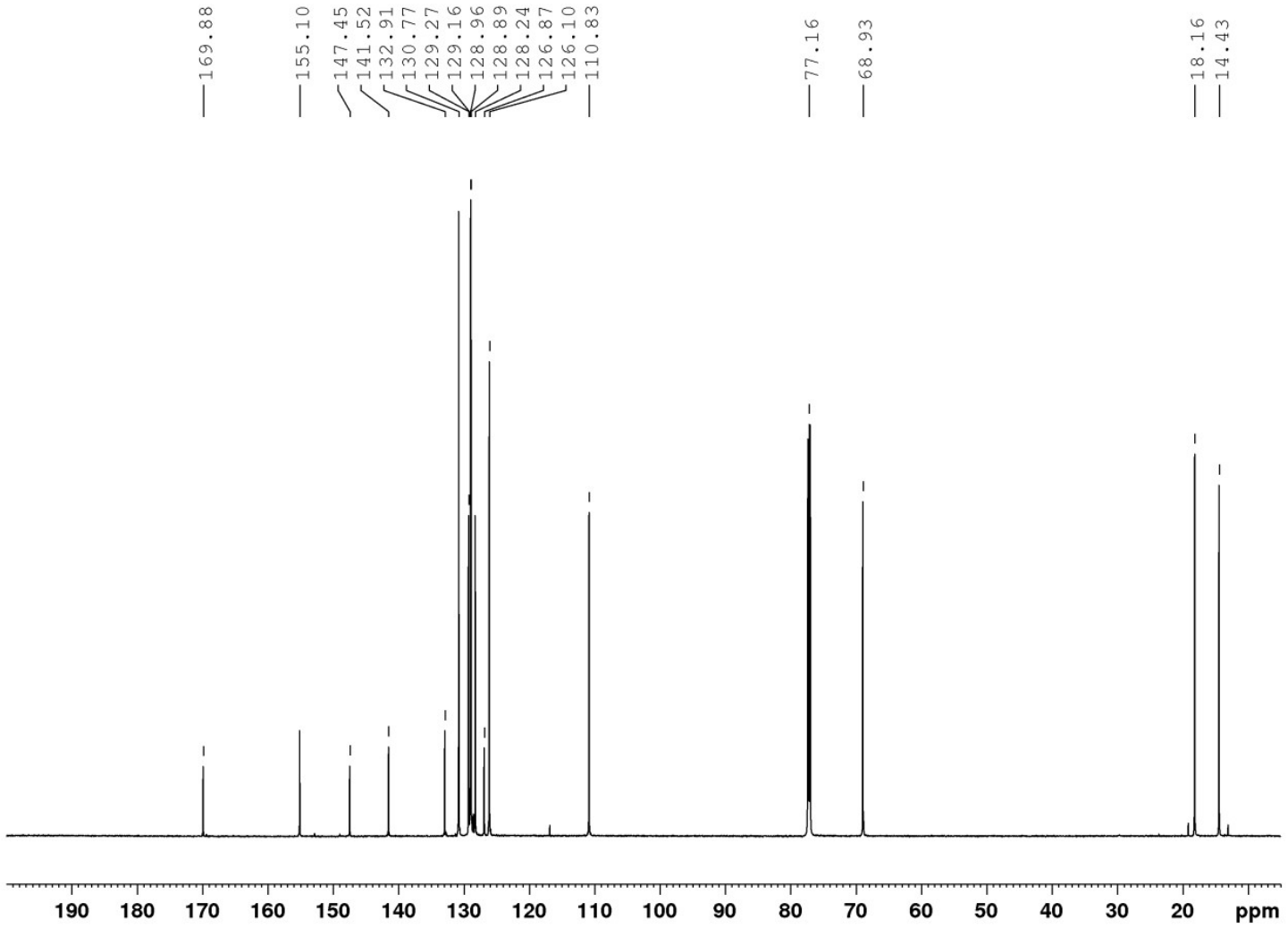

Figure S43. ^{13}C NMR spectrum of **5** (175 MHz, $CDCl_3$).

4.4 NMR spectra of **6**

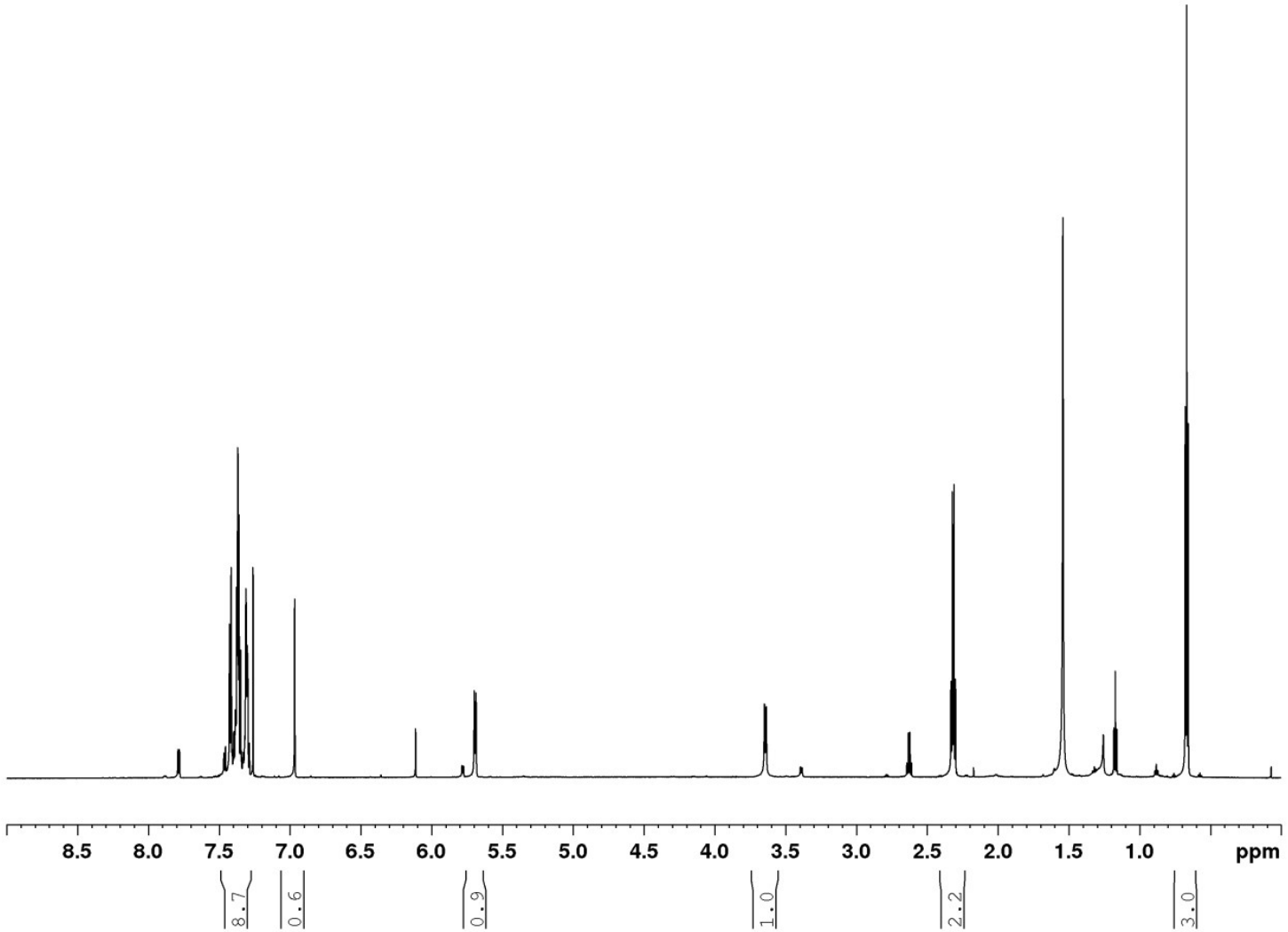

Figure S44. ^{1}H NMR spectrum of **6** (700 MHz, $CDCl_3$).

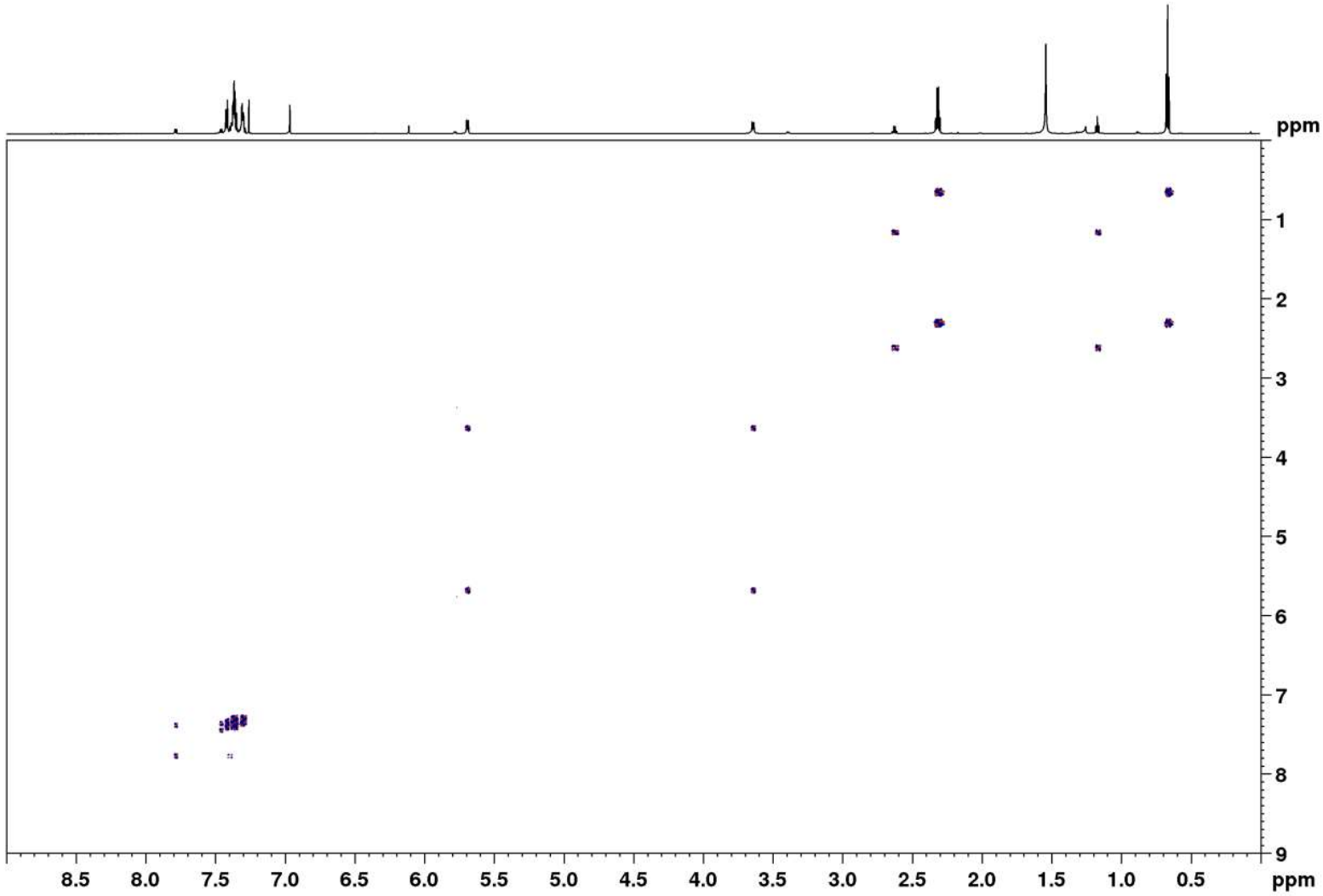

Figure S45. DQF-COSY spectrum of **6** (700 MHz, $CDCl_3$).

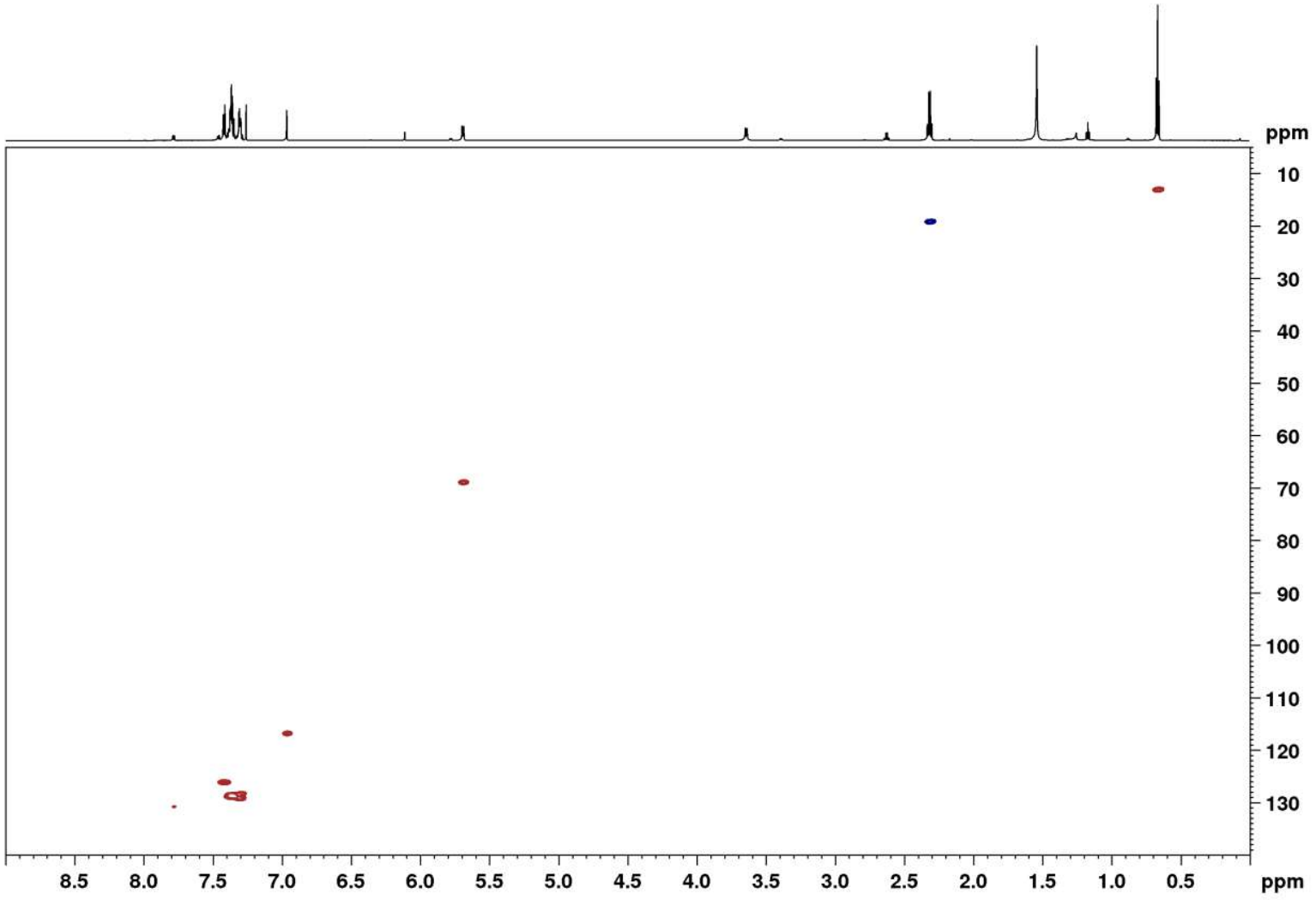

Figure S46. HSQC spectrum of **6** (700 MHz, $CDCl_3$).

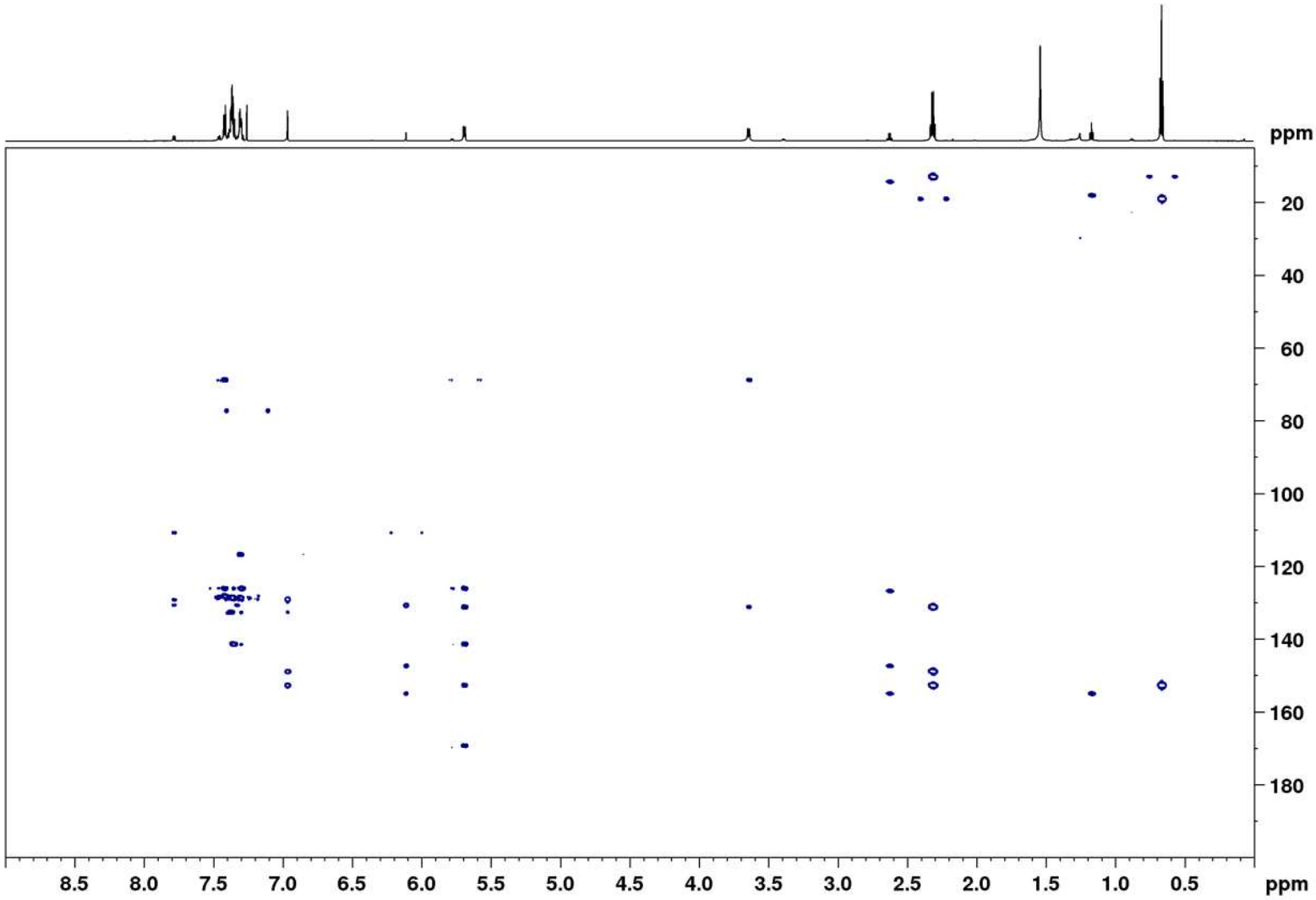

Figure S47. HMBC spectrum of **6** (700 MHz, $CDCl_3$).

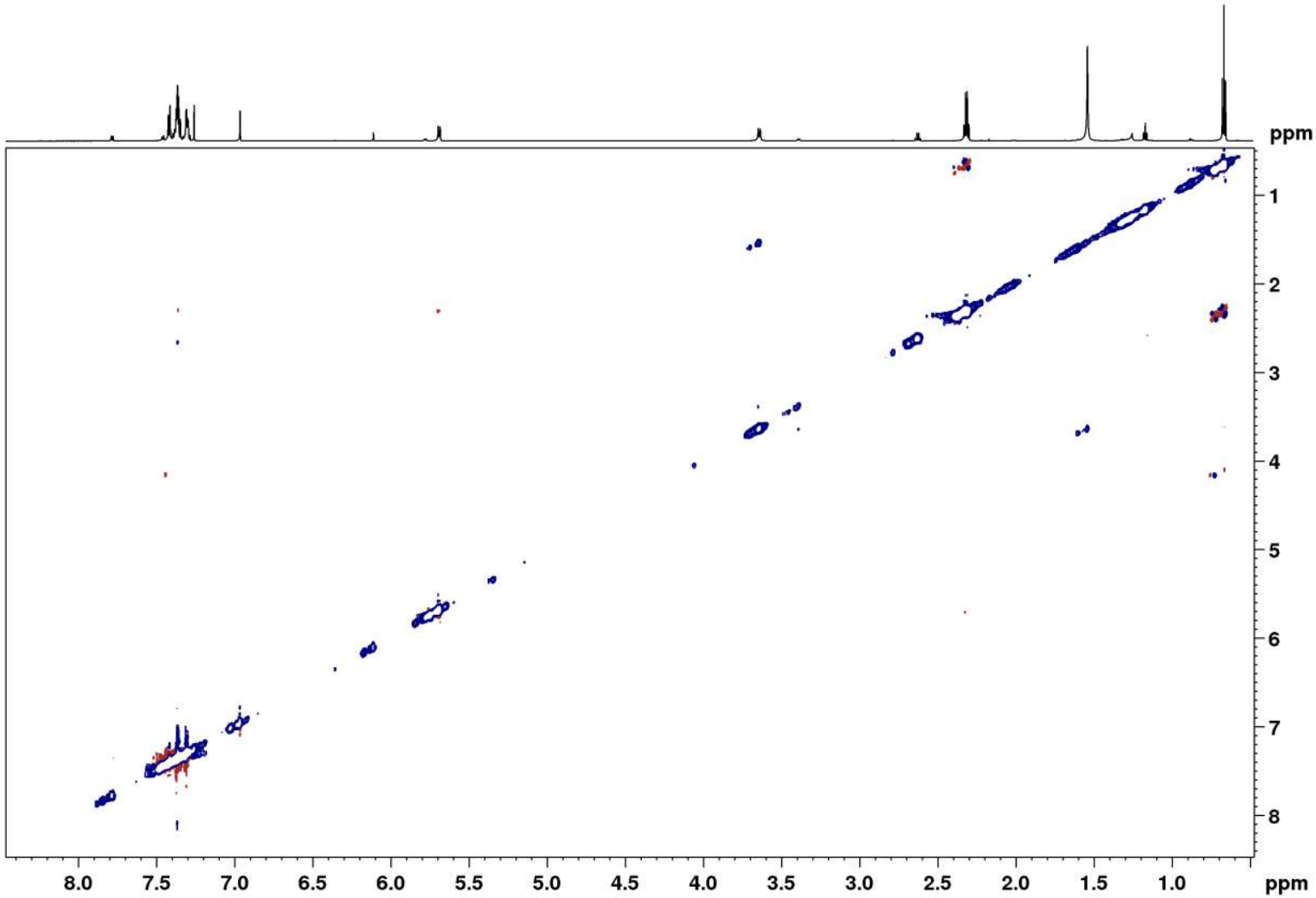

Figure S48. ROESY spectrum of **6** (700 MHz, $CDCl_3$, 300 ms).

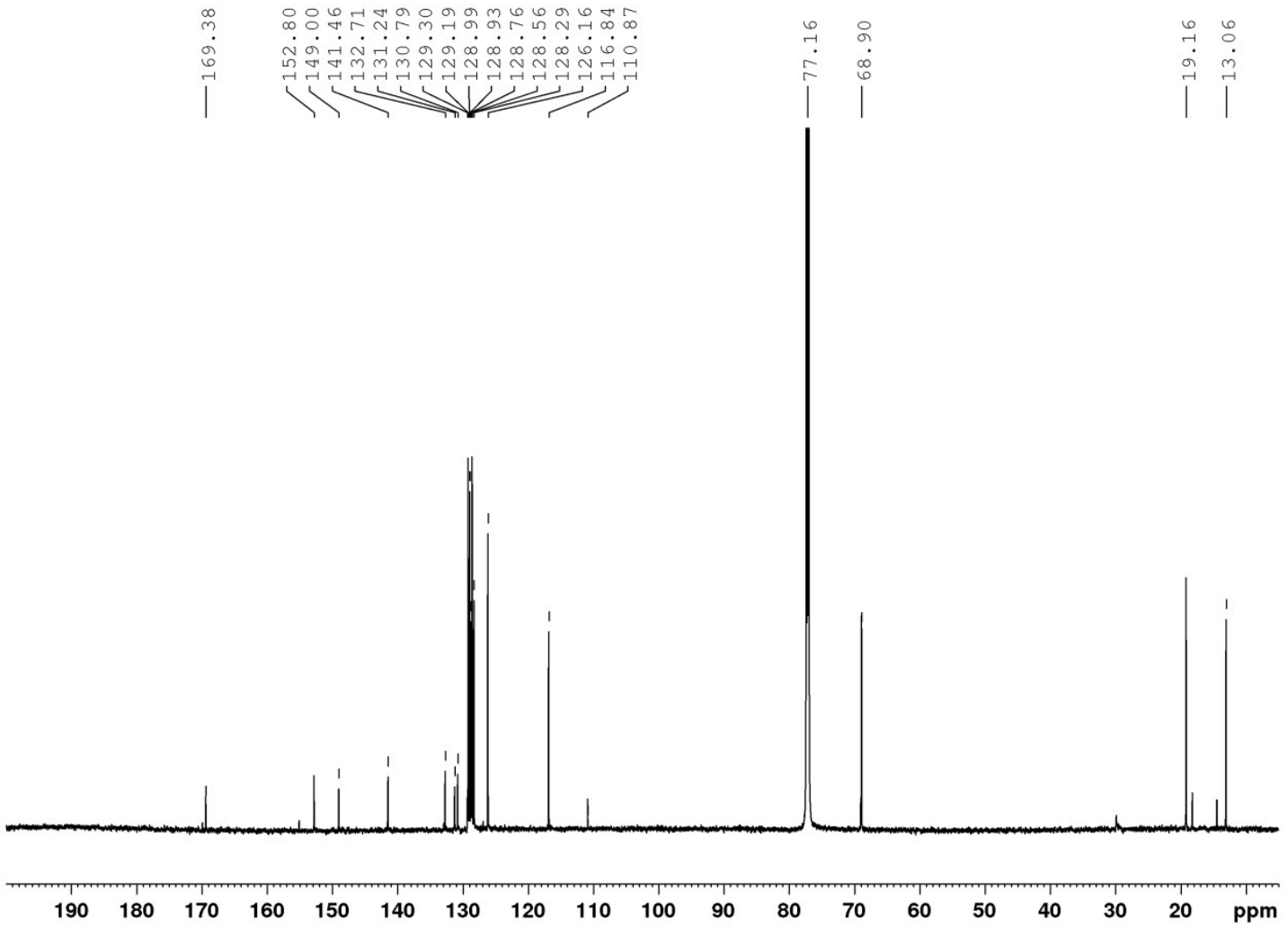

Figure S49. ^{13}C NMR spectrum of **6** (175 MHz, $CDCl_3$).

4.5 NMR spectra of **7**

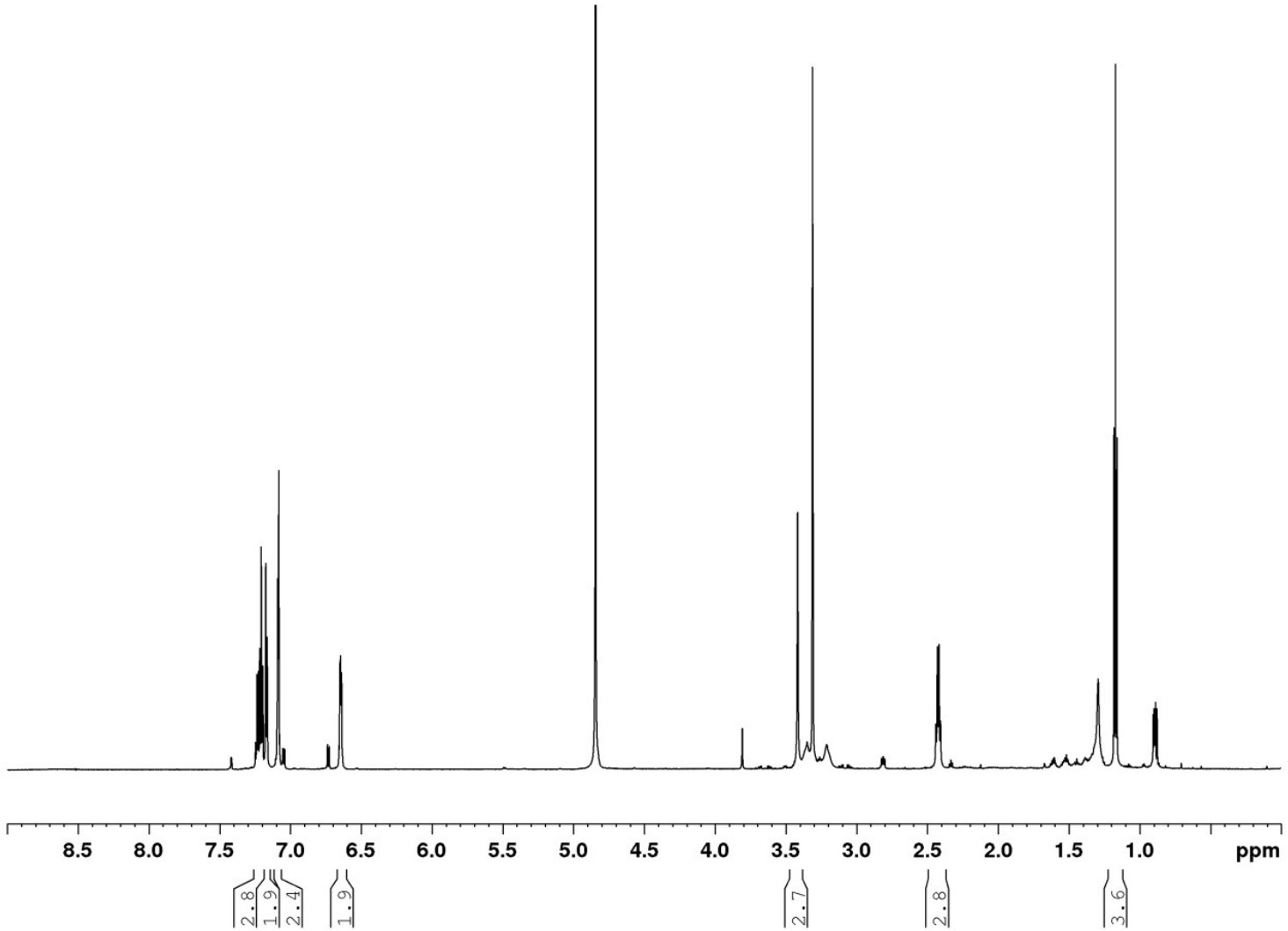

Figure S50. ^{1}H NMR spectrum of **7** (700 MHz, CD_3OD).

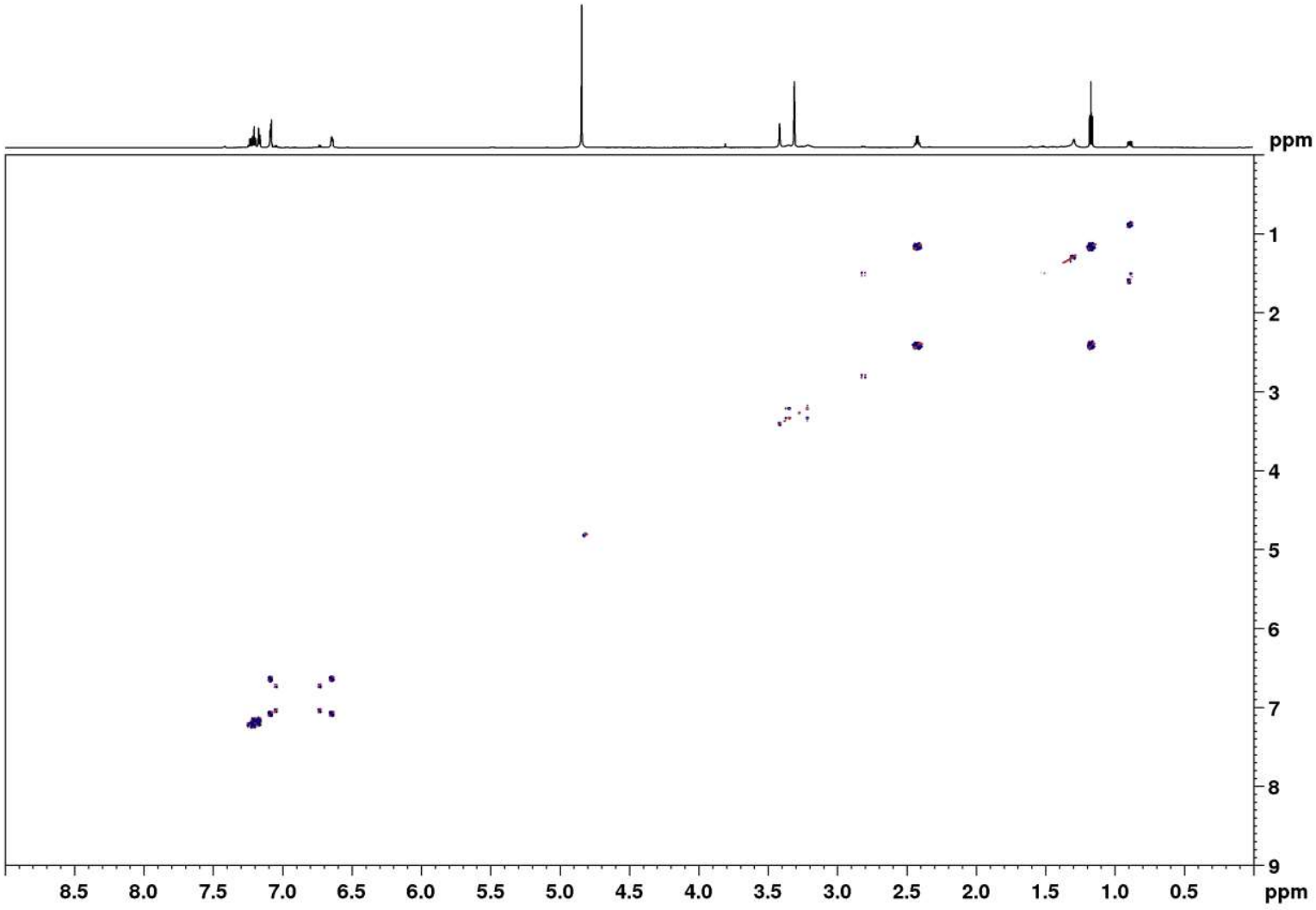

Figure S51. DQF-COSY spectrum of **7** (700 MHz, CD_3OD).

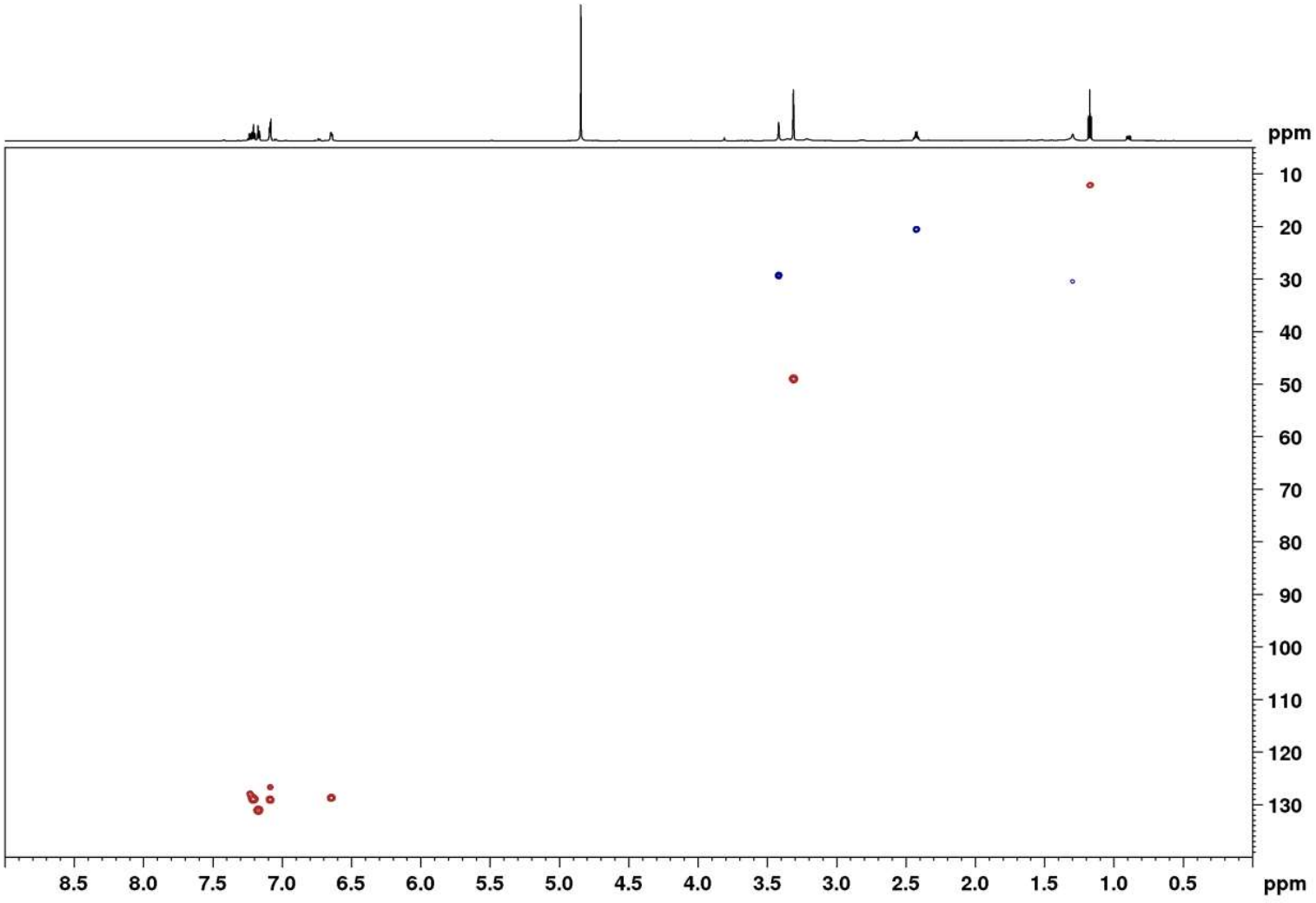

Figure S52. HSQC spectrum of **7** (700 MHz, CD_3OD).

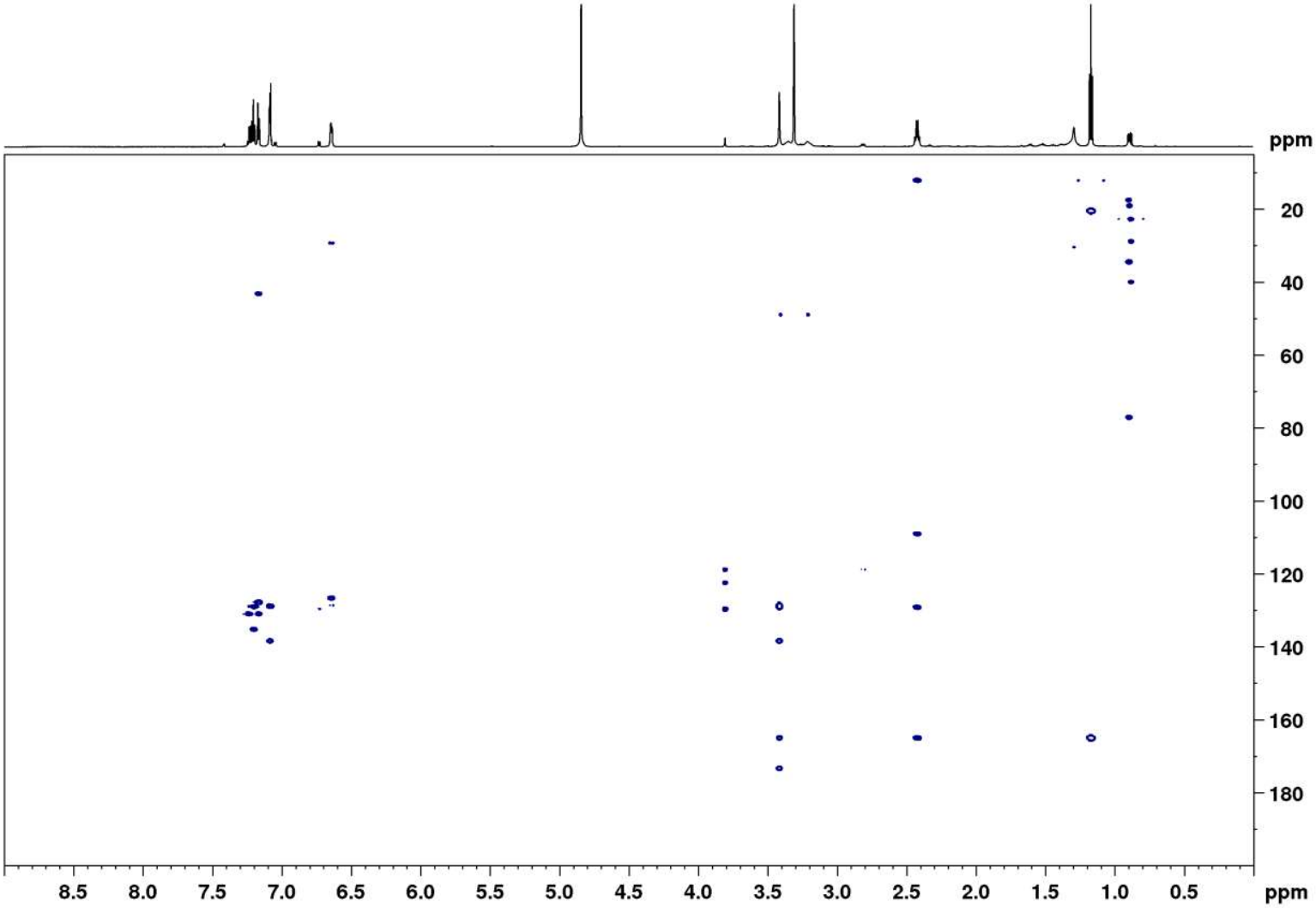

Figure S53. HMBC spectrum of **7** (700 MHz, CD_3OD).

4.6 NMR spectra of **8**

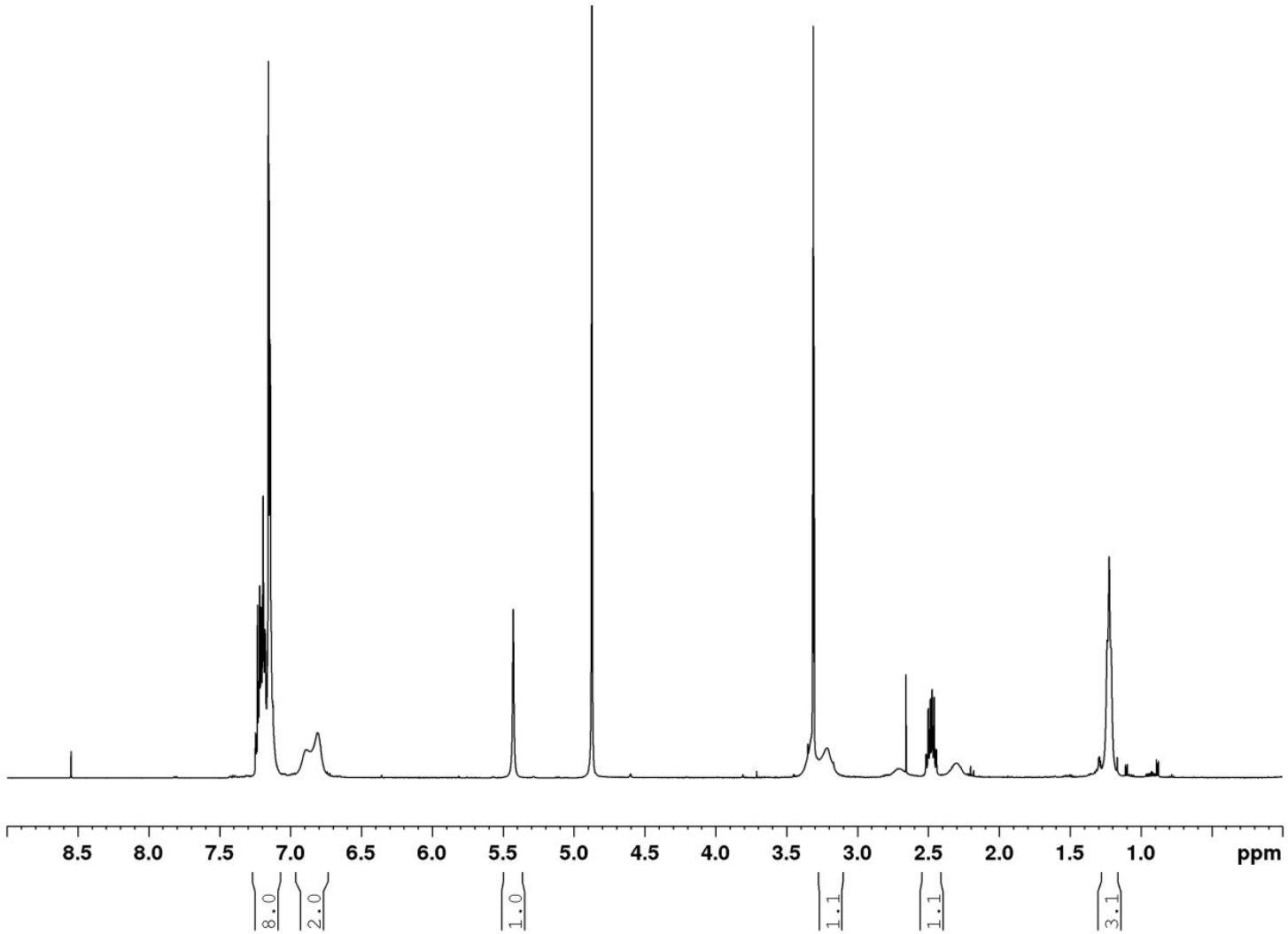

Figure S54. ^{1}H NMR spectrum of **8** (500 MHz, CD_3OD).

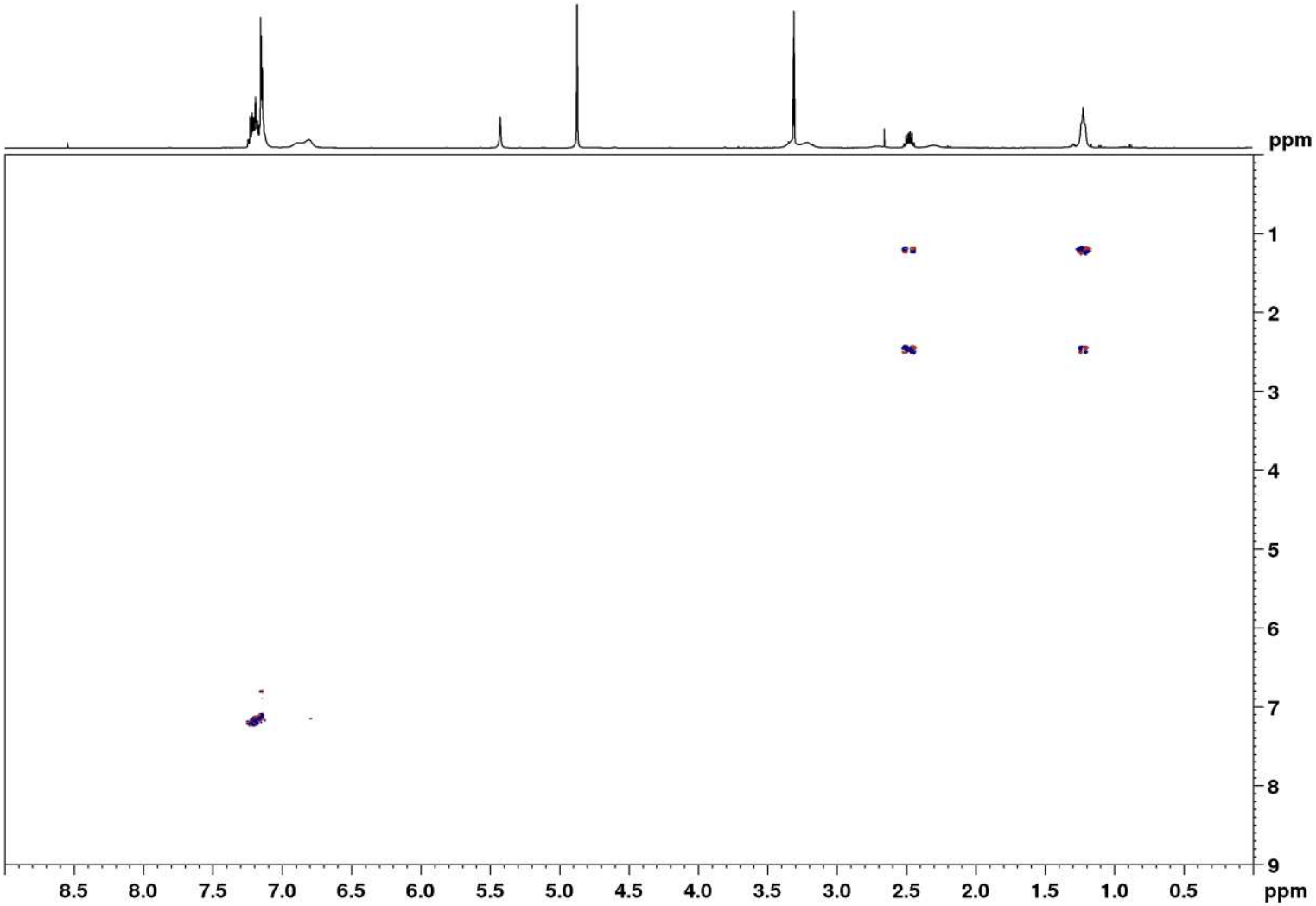

Figure S55. DQF-COSY spectrum of **8** (500 MHz, CD_3OD).

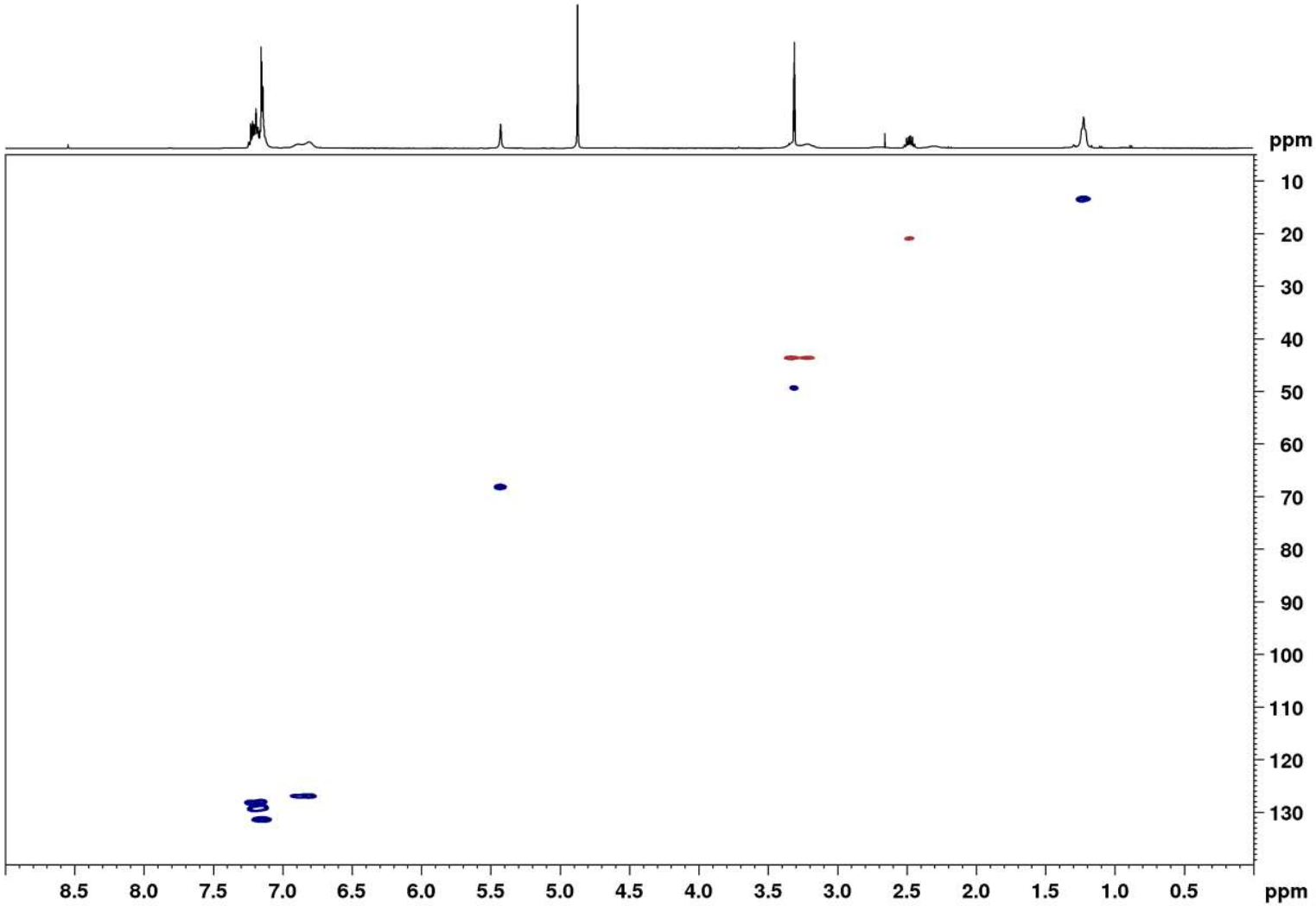

Figure S56. HSQC spectrum of **8** (500 MHz, CD_3OD).

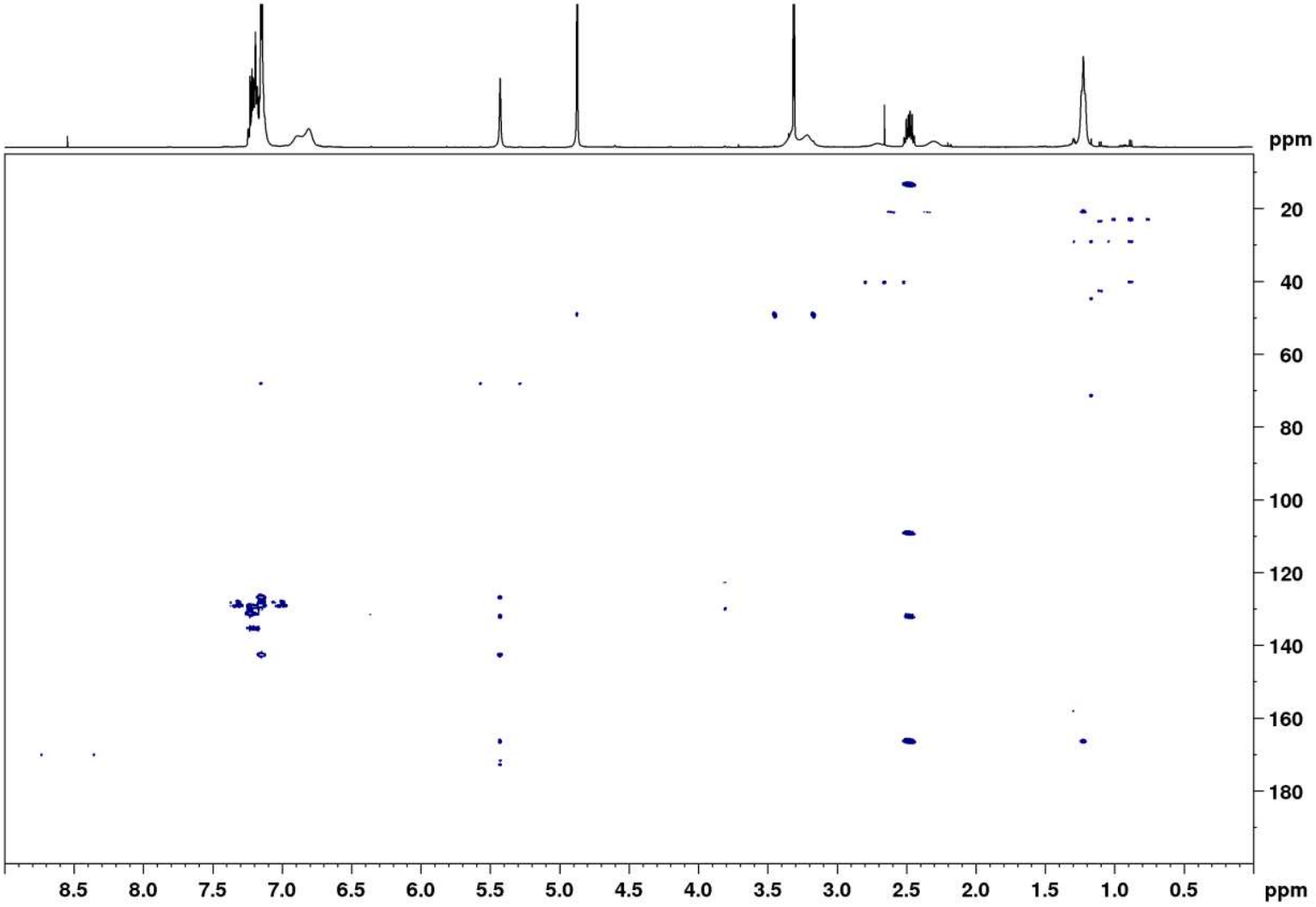

Figure S57. HMBC spectrum of **8** (500 MHz, CD_3OD).

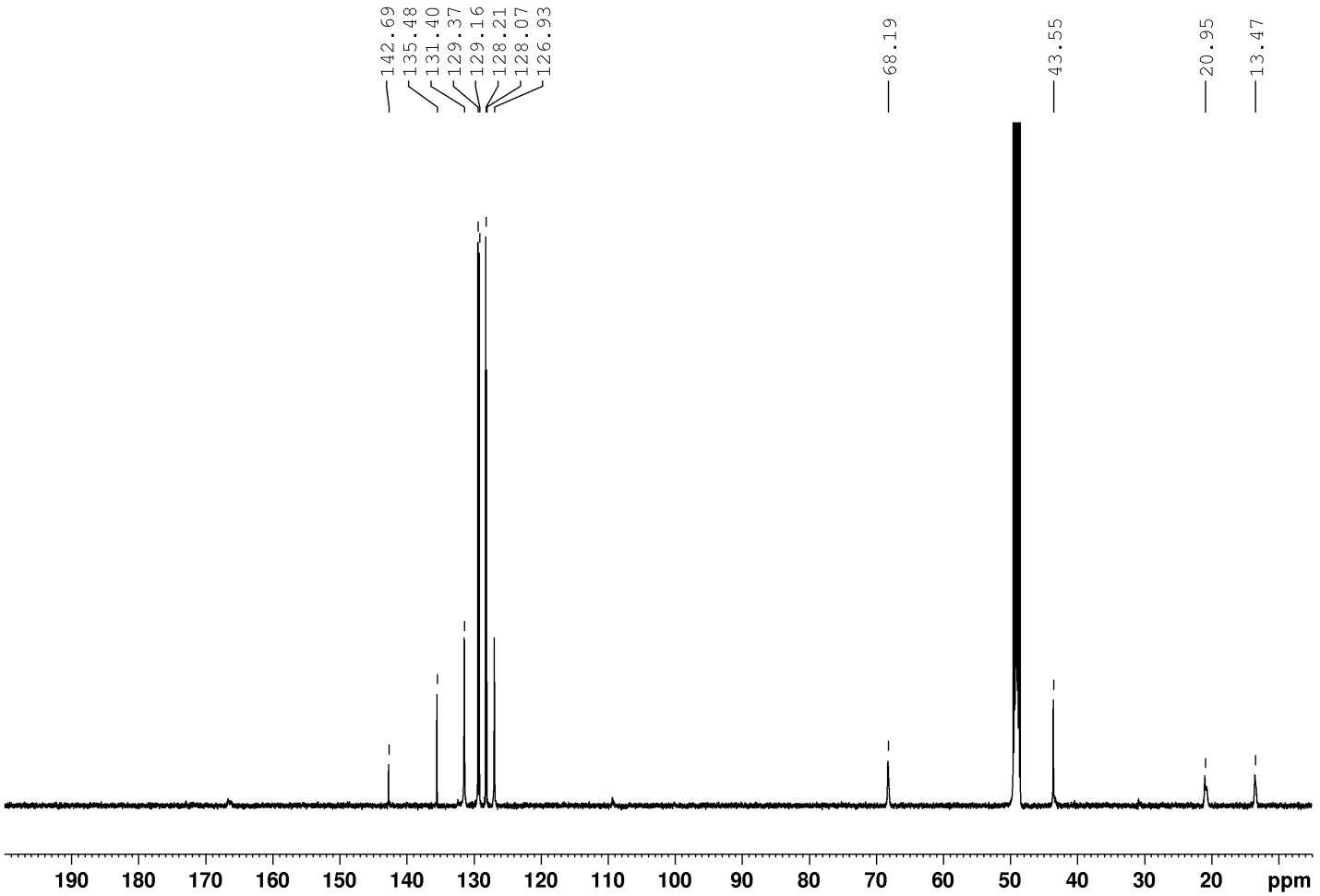

Figure S58. ^{13}C NMR spectrum of **8** (125 MHz, CD_3OD).

5. References

1 Dong, C., Flecks, S., Unversucht, S., Haupt, C., van Pée, K.-H., Naismith, J.H. (2005) Tryptophan 7-halogenase (PrnA) structure suggests a mechanism for regioselective chlorination. *Science (New York, N.Y.)*, **309** (5744), 2216–2219.

2 Henikoff, S. and Henikoff, J.G. (1992) Amino acid substitution matrices from protein blocks. *PNAS*, **89** (22), 10915–10919.

3 D'Agostino, P.M., Seel, C.J., Gulder, T., Gulder, T. (2021) *(Bio-)Synthesis of the Aquatic Phytotoxin Cyanobacterin – A Paradigm for Furanolide Core Structure Assembly*.

4 Neumann, P., Weidner, A., Pech, A., Stubbs, M.T., Tittmann, K. (2008) Structural basis for membrane binding and catalytic activation of the peripheral membrane enzyme pyruvate oxidase from Escherichia coli. *PNAS*, **105** (45), 17390–17395.

5 Lee, W.C., Cheon, D., Kim, Y. (2019) *Crystal structure of KAS III from Propionibacterium acnes*.

6 Hou, J., Chruszcz, M., Zheng, H., Cooper, D.R., Chordia, M.D., Zimmerman, M.D., Anderson, W.F., Minor, W. (2014) *Beta-ketoacyl-(acyl carrier protein) synthase III-2 (FabH2) from Vibrio cholerae soaked with Acetyl-CoA*.